

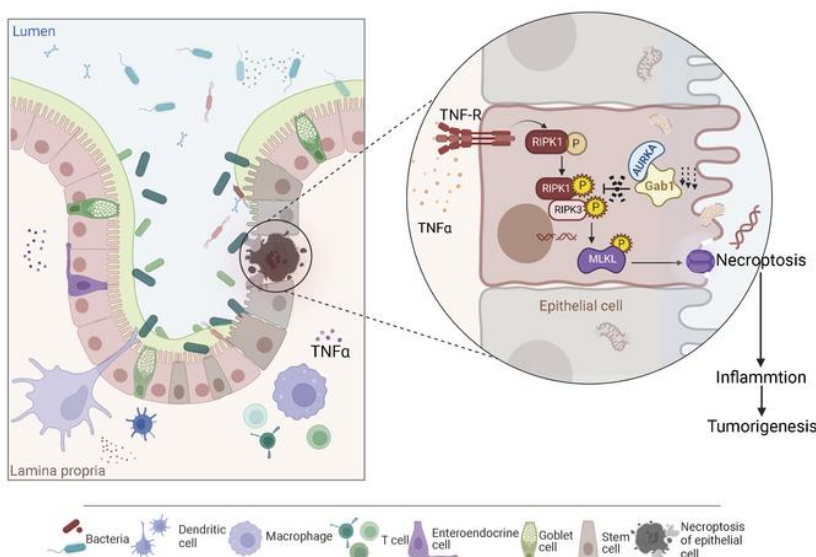
Epithelial Gab1 calibrates RIPK3-dependent necroptosis to prevent intestinal inflammation

Jiaqi Xu, ... , Zhinong Jiang, Xue Zhang

JCI Insight. 2023. <https://doi.org/10.1172/jci.insight.162701>.

Research In-Press Preview **Gastroenterology** **Inflammation**

Graphical abstract



Find the latest version:

<https://jci.me/162701/pdf>



1 **Epithelial Gab1 calibrates RIPK3-dependent necroptosis to**
2 **prevent intestinal inflammation**

3 Jiaqi Xu^{1,7}, Shihao Li^{2,7}, Wei Jin^{3,7}, Hui Zhou², Tingting Zhong¹, Xiaoqing
4 Cheng¹, Yujuan Fu¹, Peng Xiao⁴, Hongqiang Cheng⁵, Di Wang⁶, Yuehai Ke²,
5 Zhinong Jiang^{1*} & Xue Zhang^{2*}

6 1. Department of Pathology, Sir Run Run Shaw Hospital, Zhejiang University School of
7 Medicine, Hangzhou 310058, China

8 2. Department of Pathology and Pathophysiology, and Department of Respiratory Medicine
9 of Sir Run Run Shaw Hospital, Zhejiang University School of Medicine, Hangzhou 310058,
10 China

11 3. Department of General Surgery, Sir Run Run Shaw Hospital, Zhejiang University School
12 of Medicine, Hangzhou 310058, China

13 4. Department of Gastroenterology, Sir Run Run Shaw Hospital, Zhejiang University
14 School of Medicine, Hangzhou 310058, China

15 5. Department of Pathology and Pathophysiology, and Department of Cardiology of Sir Run
16 Run Shaw Hospital, Zhejiang University School of Medicine, Hangzhou 310058, China

17 6. Institute of Immunology and Sir Run Run Shaw Hospital, Zhejiang University School of
18 Medicine, Hangzhou 310058, China

19 7. These authors contributed equally: Jiaqi Xu, Shihao Li and Wei Jin.

20 * Address correspondence to: Xue Zhang, Room A312, Zhejiang University School of
21 Medicine, 866 Yuhangtang Road, Hangzhou 310058, China; Phone: 86.0571.88208583;
22 Email: zhangxue@zju.edu.cn. Or to Zhinong Jiang, Sir Run Run Shaw Hospital, 3
23 Qingchun East Road, Hangzhou 310058, China; Phone: 86.0571.86090073; Email:
24 3200039@zju.edu.cn.

25 **Conflict of interest**

26 The authors have declared that no conflict of interest exists.

27

28

29

30 **Abstract**

31 As a hallmark for inflammatory bowel disease (IBD), elevated intestinal
32 epithelial cell (IEC) death compromises the gut barrier, activating inflammatory
33 response and triggering more IEC death. However, the precise intracellular
34 machinery that prevents IEC death and break this vicious feedback remains
35 largely unknown. Here, we report that Gab1 expression is decreased in patients
36 with IBD and inversely correlated with IBD severity. Gab1 deficiency in intestinal
37 epithelial cells accounts for the exacerbated colitis induced by dextran sodium
38 sulfate (DSS) owing to sensitizing IECs to RIPK3-mediated necroptosis, which
39 irreversibly disrupted homeostasis of the epithelial barrier and promoted
40 intestinal inflammation. Mechanistically, Gab1 negatively regulates necroptosis
41 signaling through inhibiting the formation of RIPK1/RIPK3 complex in response
42 to TNF- α . Importantly, administration of RIPK3 inhibitor reveals a curative effect
43 in epithelial Gab1-deficient mice. Further analysis indicates mice with Gab1
44 deletion are prone to inflammation associated colorectal tumorigenesis.
45 Collectively, our study defines a protective role for Gab1 in colitis and colitis-
46 driven colorectal cancer through negatively regulating RIPK3-dependent
47 necroptosis, in which may serve as an important target to fine-tune necroptosis
48 and intestinal inflammation-related disease.

49

50

51

52

53

54

55

56

57

58

59

60 **Introduction**

61 Inflammatory bowel disease (IBD), typically categorized as ulcerative colitis
62 (UC) and Crohn's disease (CD), is a group of chronic relapsing inflammatory
63 disorders that affect the gastrointestinal (GI) tract in human (1, 2). Recent
64 advances highlight the central role of intestinal epithelial cells (IECs) in initiation
65 and exacerbation of IBD (3-6). IECs linked by tight junctions serve as physical
66 and biochemical barrier which facilitate host-microorganism interactions to
67 orchestrate mucosal immunity ranging from tolerance to anti-pathogen
68 response (7, 8). However, intestinal epithelial barrier breach leads to intestinal
69 hyper-permeability and microbial invasion, followed by immune activation,
70 cytokine release and mucosal inflammation, in which triggers more IEC death
71 and barrier defect, perpetuating further inflammation and thus forming a vicious
72 cycle in IBD development (9, 10).

73 IECs undergo dynamic cell turnover, necessitating a tightly regulated
74 mechanism between proliferation and cell death to safeguard intestinal barrier
75 function, wherein aberrant cell death in intestinal epithelium is a hallmark both
76 in IBD patients and mouse colitis models (11, 12). Recently, the regulated
77 necrotic cell death, namely necroptosis, has been receiving emerging attention
78 as a newly identified type of epithelial cell death regulating intestinal
79 homeostasis and inflammation (13-15). Necroptosis is a form of lytic, non-
80 apoptotic programmed cell death triggered by pro-death and innate immune
81 signals, such as TNF- α , IFNs and pathogen-associated molecular patterns
82 (PAMPs) (16, 17). The initiation of necroptosis involves the activation of protein
83 kinases receptor-interaction protein kinase 1 and 3 (RIPK1 and RIPK3), which
84 subsequently results in phosphorylation and oligomerization of mixed lineage
85 kinase-like protein (MLKL) to assemble membrane pores (18), ultimately lead
86 to the release of damage-associated molecular patterns (DAMPs) including IL-
87 1 α and alarmin high mobility group box 1 (HMGB1) (19-21). A number of genetic
88 studies revealed that mice with genetic ablation of *Caspase-8*, *Fadd* or *Setdb1*
89 in IECs developed spontaneous ileitis and colitis owing to sensitizing cells to

90 RIPK3-mediated necroptosis (22-24). Moreover, clinical evidence of aberrant
91 RIPK3 activation and necroptotic cell death has been reported in pediatric and
92 adult IBDs (22, 25, 26). However, how IEC necroptosis is negatively regulated
93 in IBD development remains elusive to date. Therefore, it is of great importance
94 to dissect negative regulation of the necroptosis to maintain intestinal barrier
95 homeostasis and optimal immune response.

96 The Grb2-associated binder 1 (Gab1) is an adaptor protein originally
97 identified downstream of growth factor and cytokine receptors including EGFR,
98 insulin receptor and c-Met (27, 28), thus participates in governing diverse
99 biological events including cell proliferation, development and angiogenesis.
100 Recent advances demonstrate the essential role for Gab1 in maintaining lung
101 surfactant homeostasis, regulating acute lung inflammation and chronic
102 asthmatic inflammation (29, 30), as well as controlling tissue repair process
103 including pulmonary and liver fibrosis (31, 32). In addition, cardiac Gab1
104 deletion leads to heart failure in aged mice associated with cardiomyocytes
105 apoptosis (33), in which apoptosis is considered immunologically silent and
106 restricting the spread of inflammation (11). Nevertheless, the
107 pathophysiological functions of epithelial Gab1 in cell death under conditions of
108 intestinal inflammation remains largely unknown.

109 In this study, we demonstrated that Gab1 expression is strikingly decreased
110 in IBD patients as well as mouse colitis model. **Deletion of Gab1 in epithelial**
111 **cells renders mice susceptible to DSS-induced colitis by perpetuating RIPK3-**
112 **dependent necroptosis.** Consistently, administration of RIPK3 inhibitor showed
113 significantly alleviation of colitis in Gab1-deficient mice. Furthermore, epithelial
114 Gab1-deficient mice displayed aggravated colorectal cancer driven by chronic
115 colitis. Together, our findings underscore that Gab1 acts as a critical
116 determinant for IEC necroptosis and intestinal inflammation, thus may providing
117 new insights into therapeutic strategy for IBD treatment.

118

119

120 **Results**

121 **Gab1 expression is decreased in IBD.**

122 To establish the correlation of Gab1 with IBD progression, we analyzed the
123 database of human samples from patients with UC or CD (34). The results
124 showed that *Gab1* was dramatically down-regulated in intestinal mucosa from
125 patients with active UC and CD compared with the control group (Figure 1A),
126 while *Gab1* was moderately decreased in UC and CD patients with remission
127 (Supplemental Figure 1A). Next, the reduction of Gab1 protein was confirmed
128 in biopsy specimens from patients with active UC and CD by
129 Immunohistochemical (IHC) and immunofluorescence staining (Figure 1, B and
130 C, Supplemental Figure 1B). In contrast, the expression of homologous family
131 protein Gab2 was comparable in the three groups of mucosal biopsies
132 (Supplemental Figure 1C). Moreover, we found that Gab1 expression was
133 markedly lower in severe IBD patients than that in mild ones (Figure 1D). *Gab1*
134 mRNA level was negatively correlated to the values of Mayo score in patients
135 with UC (Figure 1E), and the expression of pro-inflammatory cytokines in
136 patients with UC or CD (Figure 1, F and G), indicating that Gab1 was inversely
137 correlated with IBD progression.

138 Similar to the observations in human IBD, immunofluorescence staining and
139 Western blotting also revealed the decrease of Gab1 protein in DSS-induced
140 colitis mouse model, while the expression of Gab2 and Gab1-binding protein
141 Shp2 was unaltered (Figure 2, A and B). Next, intestinal epithelial cells (IECs)
142 and CD11b⁺ myeloid cells were further isolated for immunoblotting. As shown
143 in Figure 2C and D, Gab1 was mainly decreased in IECs but not CD11b⁺
144 myeloid cells upon DSS treatment.

145 To further verify the reduction of Gab1 in human IECs, we utilized a single-
146 cell RNA-sequencing dataset of human colonic crypts from immunomodulatory-
147 naive patients with UC and healthy controls (35). The results revealed the
148 distinct cell cluster profiling in colonic crypts isolated from inflamed areas of UC
149 patients compared with healthy controls (Figure 2E and Supplemental Figure 2,

150 A-C). UMAP plots showed differential distribution and apparent differences of
151 *Gab1* expression in these cell clusters (Figure 2F), in which *Gab1* is
152 predominantly decreased in colonocytes rather than other IEC subpopulations
153 and immune cells in inflamed group versus non-inflamed and healthy controls
154 (Figure 2, F and G, and Supplemental Figure 2D). These findings indicate that
155 decreased *Gab1* expression in IECs was correlated with intestinal inflammation
156 in both human and mice.

157

158 **Epithelial *Gab1* deficiency renders mice susceptible to DSS-induced**
159 **colitis**

160 To unravel the *in vivo* role of epithelial *Gab1* in colitis, we first generated
161 intestinal epithelium-specific *Gab1* knockout (*Gab1^{IEC} KO*) mice. Conditional
162 deletion of *Gab1* was confirmed by genotyping and Western blot analysis
163 (Supplemental Figure 3, A-C). These mice have no apparent gross phenotypes
164 compared with their littermate controls. Also, no significant difference was found
165 in the relative expression of mucins, antimicrobial peptides or stem cell
166 associated genes in *Gab1^{IEC} KO* mice (Supplemental Figure 4).

167 Then we induced colitis mouse model by administrating 3% DSS for 7 days.
168 Compared with *Gab1^{fl/fl}* littermates, *Gab1^{IEC} KO* mice exhibited exacerbated
169 colitis, as exemplified by more severe weight loss, diarrhea, rectal bleeding
170 (Figure 3A) as well as enhanced colon shortening and spleen swelling on day
171 7 when they were sacrificed (Figure 3, B and C). Consistent with these findings,
172 histology analysis revealed that epithelial *Gab1* deficiency led to more
173 extensive disruption of the mucosal epithelium and inflammatory infiltration
174 triggered by DSS (Figure 3D). Also, there was a decrease in the number of
175 goblet cells in *Gab1^{IEC} KO* colonic epithelium compared with controls upon DSS
176 treatment (Figure 3E). When challenged with 4% DSS, *Gab1^{IEC} KO* mice
177 manifested significantly diminished survival rate compared with *Gab1^{fl/fl}* mice
178 (Figure 3F).

179 To further verify the impact of myeloid *Gab1* deficiency on colitis development,

180 myeloid-specific *Gab1* knockout mice (*Gab1^{My}* KO) were subsequently
181 generated (Supplemental Figure 3, D and E). *Gab1^{My}* KO mice and their
182 littermates were also subjected to DSS treatment as described above. Upon
183 DSS induction, *Gab1^{My}* KO mice displayed comparable colitis-induced
184 macroscopic changes (Figure 3G and Supplemental Figure 5) and
185 histopathological damage with *Gab1^{f/f}* mice (Figure 3H). Taken together, these
186 findings define a predominant role of *Gab1* in IEC, rather than in myeloid cells,
187 in protecting mice from DSS-induced colitis.

188

189 ***Gab1* deficiency in IEC exacerbates the inflammatory responses**

190 To gain insight into the changes in biological processes and pathways caused
191 by *Gab1* deletion, we subsequently performed RNA-sequencing analysis
192 (RNA-seq) using colon tissues obtained from *Gab1^{IEC}* KO and *Gab1^{f/f}* mice with
193 a 7-day DSS treatment. A total of 1128 differentially expressed genes (DEGs),
194 including 835 upregulated and 293 downregulated genes, were shown as
195 volcano plots compared with the controls (Figure 4A). Moreover, GO analysis
196 for biological processes highlighted that DEGs were mostly enriched in
197 inflammation-related terms, programmed cell death and cell junction
198 disassembly (Figure 4B). Meanwhile, clustered heatmap diagram illustrated
199 that *Gab1*-deficient colons presented a pronounced bowel inflammatory
200 signature with high expression levels of IBD-related cytokines, chemokines,
201 inflammatory markers including *Il1b*, *Il6*, *Cxcl2*, *Saa3* (Figure 4C). The
202 transcriptome sequencing data was further validated by qPCR and ELISA.
203 Consistent with RNA-seq results, the expression of pro-inflammatory cytokines
204 as well as chemokines and antimicrobial peptides were elevated in *Gab1*-
205 deficient colon tissues (Supplemental Figure 6). Substantial increase of IL-1 β
206 and IL-6 protein was also observed in *Gab1*-deficient colonic supernatant
207 (Figure 4D). Similarly, immunofluorescence staining showed obviously
208 increased accumulation of CD45 $^{+}$ immune cells, F4/80 $^{+}$ macrophages and
209 Ly6G $^{+}$ neutrophils in colonic sections of epithelial *Gab1*-deficient mice (Figure

210 4, F-H). Also, fluorescence-activated cell sorting (FACS) confirmed the
211 significant increase in the frequencies of colon-infiltrating immune cells (CD45⁺),
212 neutrophils (CD11b⁺Ly6G⁺) and inflammatory macrophages (Ly6C^{hi}CX3CR1^{int})
213 in Gab1^{IEC} KO mice, whereas the frequencies of CD4⁺ T cells and CD8⁺ T cells
214 were similar between two groups (Figure 4E and Supplemental Figure 7). Taken
215 together, these results indicate that epithelial Gab1 deficiency facilitates
216 inflammatory cell infiltration and aggravates colonic inflammation in colitis
217 microenvironment.

218

219 **Gab1 maintains intestinal epithelial integrity through restricting aberrant**
220 **necroptosis**

221 It has been reported that patients with IBD and mice with experimental colitis
222 involve an abnormal intestinal barrier (9, 35, 36). To investigate if Gab1 affects
223 intestinal barrier function in DSS-induced colitis, FITC-Dextran in the serum
224 was determined on day 7 after DSS treatment. As shown in Figure 5A, Gab1^{IEC}
225 KO mice displayed higher serum FITC-dextran concentrations compared with
226 the controls upon DSS treatment, while two groups of mice displayed similar
227 epithelial permeability without DSS induction, indicating that Gab1 is required
228 for maintaining mucosal permeability in inflammatory environment. Tight
229 junction protein ZO-1, an indicator of the colonic epithelial integrity, localizes to
230 the cell border in IECs in steady state (37). In line with increased FITC-dextran
231 permeability, we also observed considerable loss and compromised
232 organization of ZO-1 in Gab1-deficient epithelium following DSS treatment
233 (Figure 5B).

234 Dysregulated cell death in intestinal epithelium leads to epithelial barrier
235 breach, dysbiosis and systemic spread of pathogen, which is commonly
236 observed both in IBD patients and preclinical colitis models (11, 38). Moreover,
237 our GO analysis data underscored the critical role of Gab1 in the regulation of
238 DEGs involved in the programmed cell death (Figure 4B). Hence, we evaluated
239 IEC death in this model by the TUNEL assay, which detects apoptosis and other

types of cell death (39). Compared with Gab1^{fl/fl} littermates, TUNEL-positive epithelial cells were dramatically increased in Gab1-knockout crypts challenged by DSS (Figure 5, C and D). By contrast, there was a minimal number of cleaved caspase3-positive epithelial cells upon DSS treatment, and no significance was found between two groups of mice (Figure 5, E and F). Also, immunoblotting assay revealed that the level of apoptosis-related Bcl-2 family proteins (including Bcl-2, Bcl-XL and Bax), as well as caspase3 activation were not changed in Gab1^{IEC} KO mice challenged with DSS (Supplemental Figure 8A), ruling out a significant contribution of apoptosis in this model. Meanwhile, no apparent difference was observed in ferroptosis-related proteins between two groups of mice after DSS treatment, including ACSL4, GPX4 and FTH1 (Supplemental Figure 8B), suggesting that ferroptosis contributed minimally to the aggravated colitis in Gab1^{IEC} KO mice. In addition, the cleavage of GSDMD protein was comparable in the colons of two groups following DSS challenge (Supplemental Figure 8, C and D), implying the minor contribution of GSDMD-mediated pyroptosis in our context. Interestingly, colonic protein isolated from Gab1^{IEC} KO mice showed robust phosphorylation of RIPK1, RIPK3 and MLKL compared with Gab1^{fl/fl} group (Figure 5G), indicating Gab1-deficient IECs undergo enhanced necroptosis during DSS treatment. Together, these data suggest that IEC necroptosis triggered by Gab1 deficiency aggravates intestinal barrier dysfunction and bowel inflammation in DSS-induced colitis.

262 263 **Gab1 deficiency promotes IEC necroptosis and aggravates intestinal** 264 **inflammation**

265 Necroptosis, a lytic pro-inflammatory mode of cell death, occurs in which
266 effector caspases are inhibited or inactive in response to TNF- α (40). To verify
267 the mouse phenotype owing to enhanced necroptosis in Gab1^{IEC} KO was
268 controlled by TNF- α , we performed TNF blockade assay utilizing infliximab (IFX)
269 as previously described (41-43). The aggravated colitis due to epithelial Gab1

270 deficiency was rescued by IFX administration, as exemplified by significantly
271 improved macroscopic changes, colon length, as well as intestinal epithelial
272 integrity (Supplemental Figure 9, A, B and D). Histology analysis also revealed
273 that Gab1^{IEC} KO mice displayed approximate epithelial damage and
274 inflammatory infiltration compared with $\text{Gab1}^{fl/fl}$ mice after TNF neutralization
275 (Supplemental Figure 9C).

276 Next, we utilize HT29 cell line treated with a combination of T/S/Z [TNF- α (T),
277 SM-164 (S) and pan-caspase inhibitor Z-VAD-FMK (Z)], which is a well-
278 established model to study necroptosis in vitro. Immunofluorescence imaging
279 showed significantly increase of propidium iodide (PI)-positive necroptotic cells
280 in Gab1-knockdown (shGab1) HT29 cells upon T/S/Z treatment (Figure 6A).
281 Furthermore, cell viability determined by intercellular ATP was considerably
282 decreased in Gab1-knockdown cells treated with T/S/Z (Figure 6B).
283 Transmission electron microscopy (TEM) images also revealed exacerbated
284 subcellular features of necrosis-like swelling mitochondria challenged with
285 T/S/Z in Gab1-knockdown cells (Figure 6C). Intestinal epithelium death was
286 further reproduced ex vivo in the 3D mini-gut organoid culture based on
287 previous study (44, 45). As shown in Figure 6D, PI staining revealed remarkable
288 increase of necroptotic cells in Gab1^{IEC} KO mice-derived intestinal organoids
289 following T/S/Z treatment. It has been highlighted that extensive necroptosis in
290 IECs tiggers intestinal inflammation by a massive release of DAMPs, which
291 links cell death to mucosal inflammation (22, 46). Therefore, we examined the
292 levels of DAMPs (including HMGB1, IL1 family cytokines) as well as Cxcl family
293 chemokines with or without Gab1. Western blotting revealed a higher amount
294 of HMGB1 detectable in culture supernatant in Gab1-deficient cells after T/S/Z
295 treatment (Figure 6E). QPCR analysis also displayed that Gab1 deletion
296 resulted in significantly higher expression of *Il1a*, *Il1b*, *Cxcl1*, *Cxcl2* and *Cxcl8*
297 upon necroptosis stimulation (Figure 6, F and G). Consistent with above data,
298 T/S/Z-triggered cell necroptosis was significantly restrained by the
299 overexpression of Gab1, as indicated by both reduced PI-positive necroptotic

300 cells (Figure 6, H and I) and mitigated swelling of mitochondria in HT29 cells
301 (Figure 6J). Thus, these findings further support the role of Gab1 in negatively
302 regulating epithelial necroptosis in response to TNF- α .

303

304 **Gab1 negatively regulates necroptosis through interacting with RIPK3 via**
305 **AURKA**

306 The necroptosis signaling is mainly initiated by TNF- α , followed by the
307 activation of protein kinases RIPK1 and RIPK3, which subsequently
308 phosphorylate the downstream MLKL pseudokinase to induce cell membrane
309 rupture and executes necroptosis (18, 47, 48). Western blot analysis showed
310 that the phosphorylation level of RIPK1, RIPK3 and MLKL was remarkably
311 elevated in Gab1-knockdown HT29 cells following T/S/Z treatment (Figure 7A),
312 whereas overexpression of Gab1 suppressed T/S/Z induced
313 RIPK1/RIPK3/MLKL activation (Figure 7B). To dissect the underlying
314 mechanism that Gab1 negatively regulates RIPK1/RIPK3/MLKL axis, we
315 examined the interaction between Gab1 and pro-necroptotic factor RIPK3. As
316 shown in Figure 7C, endogenous Gab1 bound with RIPK3 in basal state, and
317 this association was impaired upon T/S/Z treatment in HT29 cells. Besides,
318 similar effects were observed in HEK293T cells overexpressing Gab1-Flag and
319 RIPK3-Myc plasmids, as demonstrated by co-IP (Figure 7D). The interaction of
320 Gab1 and RIPK3 was further confirmed by a pull-down assay in vitro, as
321 recombinant GST-fused Gab1 protein was able to pull down RIPK3 from
322 HEK293T cell lysates (Figures 7, E and F). Importantly, we found that Gab1
323 deficiency promotes the formation of RIPK1 and RIPK3 complex under
324 necroptotic conditions (Figure 7G), thus facilitates downstream activation of
325 necroptosis. Recent approach showed that Aurora kinase A (AURKA) is a direct
326 negative regulator of necrosome activation through binding the RIPK1/RIPK3
327 complex (49). Interestingly, AURKA was identified as binding protein of Gab1
328 by using liquid chromatography with tandem mass spectrometry (LC-MS)
329 (Supplemental Figure 10), and further confirmed by co-IP (Figure 7H). Thus,

330 we propose that Gab1 interacts with RIPK3 through AURKA, thus restrain the
331 assembly of RIPK1/RIPK3 complex. Collectively, these data indicate that Gab1
332 negatively regulates cell necroptosis by serving as a brake on RIPK1/RIPK3
333 complex formation in response to necroptotic signals.

334

335 **RIPK3 inhibition alleviates colitis in epithelial Gab1-deficient mice.**

336 We have shown that *Gab1* ablation in IECs contributed to the aggravated
337 colitis due to excessive RIPK3-dependent necroptosis. Therefore, we utilized
338 N-(6-(Isopropylsulfonyl) quinolin-4-yl) benzo[d]thiazol-5-amine (GSK'872), a
339 specific RIPK3 inhibitor (50, 51), to further validate whether uncontrolled
340 necroptosis in *Gab1^{IEC}* KO mice accounts for this phenotype. *Gab1^{fl/fl}* or
341 *Gab1^{IEC}* KO mice were subjected to a 7-day course of 3% DSS and treated with
342 either vehicle control or GSK'872 intraperitoneally. The results revealed that
343 GSK'872 treatment showed curative effects in both *Gab1^{fl/fl}* and *Gab1^{IEC}* KO
344 mice after DSS exposure. The aggravated colitis due to epithelial Gab1
345 deficiency was significantly rescued by GSK'872 administration, as exemplified
346 by DSS induced macroscopic changes (body weight loss, diarrhea, and rectal
347 bleeding) were significantly alleviated (Figure 8A). Consistently, *Gab1^{IEC}* KO
348 sacrificed on day 7 and displayed approximate colon length (Figure 8B),
349 epithelial damage, inflammatory infiltration (Figure 8C) and the number of
350 goblet cells (Figure 8D) compared with *Gab1^{fl/fl}* littermates after GSK'872
351 administration. Moreover, GSK'872 treatment significantly reduced the number
352 of TUNEL-positive epithelial cells, and the phosphorylation of RIPK3 and MLKL
353 in colon tissues triggered by DSS (Figure 8, E and F). Taken together, these
354 data indicate that hyperactivation of RIPK3 and necroptosis in IECs is primarily
355 responsible for the exacerbated colitis in *Gab1^{IEC}* KO mice.

356

357 **Gab1 expression is associated with UC therapeutic outcomes and**
358 **colorectal cancer**

359 The introduction of anti-TNF therapy in the treatment of IBD has significantly

improved the disease outcome. However, approximately 10-40% of patients do not respond to induction therapy (primary non-response) (52). Thus, we assessed the *Gab1* expression in patients before and after first anti-TNF treatment. We found that *Gab1* was dramatically upregulated in the inflamed mucosa of anti-TNF-responded UC patients after first infliximab or golimumab treatment whereas *Gab1* was comparable in infliximab-responded CD patients before and after treatment (Figure 9, A and B). Subsequently, we utilized infliximab, the chimeric mouse-human monoclonal antibody to neutralize TNF activity in mouse. Consistent with the observations in human UC, we found that the reduction of *Gab1* expression in colonic tissues was significantly rescued after anti-TNF treatment in DSS-induced colitis model (Figure 9C). These results suggested that the increasement of *Gab1* expression after treatment may predict efficient therapeutic outcomes for UC.

Considering that necroptosis is linked to inflammation, and chronic inflammation is suggested to be a high risk factor for colorectal cancer (CRC) (15, 50). Therefore, we analyzed the CRC database and found a significantly decrease of *Gab1* expression in both patients with colon adenocarcinoma (COAD) and rectal adenocarcinoma (READ) compared with normal controls (Figure 9D). Moreover, overall survival data indicated that lower *Gab1* expression related to poorer clinical outcomes (Figure 9E). Next, we used the AOM/DSS model of colitis-associated cancer (CAC) to further determine the role of *Gab1* in inflammation related tumorigenesis in vivo (Figure 9F) (53). As shown in Figure 9G-J, *Gab1^{IEC}* KO mice exhibited a significantly increased number and size of tumors in the colorectum compared with *Gab1^{f/f}* mice. H&E staining showed larger tumors formed in epithelial *Gab1*-deficient colorectum (Figure 9K). These data suggest that *Gab1* inhibits tumorigenesis driven by chronic colitis in mice, and may serve as tumor suppressor in human CRC.

In summary, our study defines a protective role for *Gab1* in intestinal inflammation through restraining epithelial cell necroptosis.

390 **Discussion**

391 Increasing evidence highlights that intestinal barrier dysfunction greatly
392 contributes to the predisposition and perpetuation of IBD (54-56). However, the
393 molecular mechanisms underlying the epithelial barrier maintenance remain
394 obscure. Herein, we defined a crucial role for Gab1 in protecting intestinal
395 barrier by preventing epithelial cell necroptosis during intestinal inflammation,
396 which provides new insights into the diagnostic and therapeutic approach for
397 IBD.

398 Intestinal epithelial cells (IECs), linked by tight junctions, form a permeable
399 barrier separating luminal microbes and mucosal immune cells to coordinate
400 an appropriate host response, ranging from tolerance to anti-pathogen
401 immunity (7, 57). Serving as the first line of defence against microbial
402 encroachment, impaired IEC function has been reported in a wide array of
403 intestinal disorders, especially in IBD (9, 58, 59). Moreover, intestinal barrier
404 dysfunction might precede the clinical diagnosis of IBD by years, invoking the
405 possibility of preventing IBD by the early and precise interventions (10). In this
406 study, our data revealed that of Gab1 is remarkably decreased in both UC and
407 CD patients, and the extent of reduction is negatively correlated with IBD
408 progression. Single-cell RNA sequencing analysis of UC patients, as well as
409 colitis mouse model, further identified that Gab1 is predominant decreased in
410 IECs, suggesting the probable role of epithelial Gab1 in disease progression.

411 Gab1 serves as adaptor protein for integrating receptor-mediated signaling
412 cascades downstream of growth factors or cytokines (27, 28). Global Gab1
413 ablation leads to embryonic lethality in mice, with profound developmental
414 defects in heart, placenta, and skin (60). Besides the well-known function for
415 Gab1, increasing evidence demonstrates that Gab1 participates in LPS-
416 induced acute lung inflammation, house dust mite (HDM)-induced asthmatic
417 inflammation and vascular inflammation, highlighting the unique role for Gab1
418 in inflammation associated diseases (29, 30, 61). Furthermore, recent study
419 indicates that Gab family proteins Gab2/3 synergistically suppress colitis

420 through controlling macrophage and CD8⁺ T cell activation (62). However, to
421 date, the role of Gab1 in intestine and intestinal inflammation remain largely
422 unknown. Considering the remarkable reduction of Gab1 in IECs we have
423 demonstrated, VillinCre-Gab1^{fl/fl} mice (Gab1^{IEC} KO) were first generated to
424 dissect the role of Gab1 in intestinal inflammation. Notably, epithelial Gab1-
425 deficient mice manifested exacerbated experimental colitis upon DSS
426 treatment. Next, RNA-sequencing data revealed excessive production of pro-
427 inflammatory cytokines, chemokines, as well as antimicrobial peptides in
428 Gab1^{IEC} KO colons. Further GO analysis underscored an enrichment of gene
429 sets responsible for programmed cell death in the colonic transcriptome of
430 Gab1^{IEC} KO mice, implicating the potential cellular process Gab1 involved
431 during colitis development.

432 Epithelium homeostasis rests on the dynamic balance of cell proliferation and
433 death, and aberrant increase of IEC death can lead to intestinal barrier
434 disruption and inflammation. The regulation of cell death in IECs is highly
435 context dependent. It has been reported that IECs undergo a series of cell
436 death triggered by IBD, including apoptosis, necroptosis, pyroptosis and
437 ferroptosis (11, 14, 63-66). Recently, as a highly pro-inflammatory mode of cell
438 death, necroptosis has been emerged as a critical player in the modulation of
439 intestinal homeostasis and inflammation that requires stringent control (15, 67,
440 68). Clinical evidence indicates necroptosis is highly active in both pediatric and
441 adult IBDs (25, 26). Consistently, genetic approaches reveals a number of gene
442 ablation, including *Fadd*, *Casp-8*, *Setdb1* leads to spontaneous ileitis due to
443 uncontrolled necroptosis but can be rescued on Ripk3^{-/-} or Mlkl^{-/-} back (3, 22,
444 23). Several studies have linked Gab1 to cell death mainly through MAPK
445 signaling. Cardiac Gab1 deletion leads to cardiomyocyte apoptosis and heart
446 failure (33) while hepatocyte Gab1 controls the balance between
447 acetaminophen-induced hepatocyte death and compensatory proliferation (69).
448 Also, enhanced autophagy in Gab1-deficient vascular endothelial cells is
449 observed in atherosclerosis. Here, we discovered a novel role for Gab1 in

450 regulating IEC necroptosis in RIPK3-dependent manner. We found Gab1
451 deficiency renders IECs susceptible to necroptosis, thereby shifting to
452 aggravated barrier disruption and intestinal inflammation during DSS
453 administration whereas other types of cell death (apoptosis, pyroptosis and
454 ferroptosis) were unchanged. Collectively, we identified, for the first time to our
455 knowledge, the novel protective role for Gab1 in restricting this lytic form of cell
456 death during intestinal inflammation.

457 Different stimuli engage necroptosis, including TNF family, Toll-like receptors,
458 and intracellular DNA/RNA sensors, with the best characterized being TNF-
459 α (70). Given that the clinical efficacy of anti-TNF- α therapy has established TNF-
460 α as a key player in IBD, we next focused on TNF- α -elicited necroptosis in our
461 study. In response to TNF- α simulation, RIPK1 can associate with RIPK3, leads
462 to autophosphorylation and assembly of a necosome complex, especially
463 when caspase-8 activation is blocked or inefficient (40). RIPK3 subsequently
464 phosphorylates the pore-forming protein MLKL to permeabilize plasma
465 membrane and release of pro-inflammatory DAMPs, such as HMGB1 (19, 20,
466 71). To elucidate the mechanism of necroptosis affected by Gab1 deficiency,
467 we utilized the human colorectal cell line HT29, which is a well-established cell
468 line used to study the molecular machinery of necroptosis. Consistent with in
469 vivo data above, we found pronounced induction of necrotic cell death in
470 Gab1-knockout group, as well as in Gab1-deficient intestinal organoids, while
471 Gab1 overexpression suppresses necroptosis upon T/S/Z treatment.
472 Mechanismly, Gab1 blocks assembly of RIPK1/RIPK3 complex depending on
473 the ability of Gab1 to bind with RIPK3, and thereby limiting the phosphorylation
474 of RIPK3 and MLKL. Moreover, pharmacologically inhibition of RIPK3
475 significantly alleviates experimental colitis with reduced inflammation in
476 Gab1^{IEC} KO mice, suggesting that hyperactivation of RIPK3 and necroptosis
477 largely contributes to exacerbated colitis in epithelial-Gab1 deficient mice.

478 Chronic colitis is considered as a high risk factor for colorectal cancer (CRC),
479 therefore we extended our studies to investigate the role for Gab1 in CAC and

480 CRC. Previous study reported that Gab1 overexpression in DLD-1 colon
481 carcinoma cells promoted tumor growth in a subcutaneous model (72), which
482 is consistent with the in vitro findings from Bai et al (73). In contrast, Liang et al
483 delineated the tumor-suppressing role for Gab1 in CRC (74). In our study, we
484 generated mice with *Gab1*-knockout in normal intestinal epithelium, followed by
485 AOM/DSS induction to mimic the progression of inflammation-associated
486 carcinogenesis. *Gab1*^{EC} KO mice exhibited a significantly increased number
487 and size of tumors in the colorectum compared with *Gab1*^{f/f} mice, suggesting
488 a protective role for Gab1 in tumorigenesis driven by chronic colitis in mice,
489 which is consistent with our bioinformatic results in CRC patients.

490 The anti-TNF monoclonal antibodies have been extensively used for patients
491 with IBD refractory to conventional medications such as corticosteroids and
492 immunomodulators (75, 76). Effective treatment improves mucosal healing,
493 reduces hospitalisations and surgeries, but unfortunately, anti-TNF treatment
494 failure is common. About 10-40% of patients do not respond to induction
495 therapy (primary non-response), and approximately 24-46% of patients have
496 secondary loss of response in the first year of treatment, even 10% of patients
497 have adverse drug effects (77). Our data revealed that *Gab1* was significantly
498 elevated in mucosal biopsies obtained from UC patients response to infliximab
499 or golimumab, while non-response group displayed minimal changes in *Gab1*
500 expression, thus providing a genetic predictor to assess clinical outcomes of
501 anti-TNF therapy in UC. However, there is only a slight rising trend of *Gab1*
502 expression in inflamed mucosa before and after treatment in infliximab-
503 responded CD patient. We speculate that this inconsistent changes of *Gab1*
504 expression occur in responders with UC and CD possibly because of the
505 dissimilarities underlying between UC and CD, while the considerable within-
506 group differences due to the sample size of CD cohort may also account for this
507 inconsistency. Currently, several RIPK1/RIPK3 inhibitors are now in clinical
508 trials for the treatment of ulcerative colitis, expecting to prevent intestinal barrier

509 breach by inhibiting IEC death and promoting resolution of inflammation (78,
510 79). Therefore, RIPK1/RIPK3 inhibitors may synergize with anti-TNF therapy to
511 achieve higher immunosuppressive effects and improved outcomes.

512 In summary, our data demonstrate Gab1 as a critical regulator in maintaining
513 epithelial barrier integrity to protect against intestinal inflammation through
514 restricting aberrant necroptosis. These findings not only elucidate a deeper
515 understanding of IBD pathogenesis by linking epithelial-Gab1 with TNF- α
516 triggered necroptosis, but also provide new therapeutic strategies for
517 personalised induction regimens to improve clinical outcomes in a more
518 effective manner.

519

520 **Methods**

521 **Human samples**

522 Clinical samples of UC and CD patient, as well as healthy individuals, were
523 obtained from Sir Run Run Shaw Hospital, Zhejiang University School of
524 Medicine, China. The diagnosis of UC or CD was based on clinical
525 characteristics, endoscopic examination, histological analysis and radiological
526 criteria. Mayo Score and SES-CD were used to assess disease severity of the
527 patients with UC and CD, respectively (80, 81). Healthy volunteers were
528 recruited based on their medical history and routine laboratory tests including
529 complete blood count (CBC) and C-reactive protein (CRP). Normal ileal and
530 colonic mucosa samples were obtained by endoscopy with the confirmation of
531 endoscopic features and histological examination. The demographic
532 information for the subjects is detailed in Supplemental Table 1. The study was
533 approved by the Medical Ethics Committee of Sir Run Run Shaw Hospital.

534

535 **Mice**

536 The Gab1^{flox/flox} mice are a gift from Prof. Gen-sheng Feng (Department of
537 Pathology, Division of Biological Sciences and Moores Cancer Center,
538 University of California, San Diego, CA, USA). Gab1^{flox/flox} mice were crossed

539 with Villin^{Cre/+} (C57BL/6 background) mice to generate IEC-conditional Gab1
540 knockout mice (VillinCre-Gab1^{f/f}, Gab1^{IEC} KO) and their littermate controls
541 (Gab1^{f/f}). Gab1^{fl/fl} mice were crossed with LysM^{Cre/+} (C57BL/6 background)
542 mice to generate myeloid cell-specific Gab1 knockout mice (LysMCre-Gab1^{f/f},
543 Gab1^{My} KO) and their littermate controls (Gab1^{f/f}). Mice were housed in specific
544 pathogen-free environment (25 °C, suitable humidity, 12-hour light/dark cycle)
545 and fed with sufficient water and food. All protocols of animal experiments were
546 approved by the Animal Care and Use Committee of the Zhejiang University
547 School of Medicine.

548

549 **Induction of colitis**

550 Mice were administrated with dextran sulfate sodium (DSS) in drinking water to
551 induce colitis as previously described (53). In brief, Eight- to ten-week-old Gab1
552 conditional-KO mice and their littermates were treated with 3% DSS (MP
553 Biomedicals) in drinking water (w/v) for 7 days and sacrificed for further study.
554 During the experiment, body weights, diarrhea and rectal bleeding were
555 monitored daily. The scores were evaluated as follows: diarrhea: 0 = well-
556 formed stools, 2 = soft and pasty stools, and 4 = watery stools; 0 = no bleeding,
557 2 = positive hemoccult, and 4 = gross bleeding.

558

559 **Single-cell RNA-seq analysis**

560 Single cell data used in this study was acquired from the Gene Expression
561 Omnibus (GEO) with accession number GSE116222 (35). A total of 11175 cells
562 from the colonic crypts of 3 UC patients and 3 healthy individuals were
563 downloaded as Raw Data for epithelial and immune cells. Data processing
564 including batch correction, doublet removal, gene annotation and cell clustering
565 was performed as previously described. After that, the Seurat R package
566 (version 2.3.2) was used to normalize expression values for total UMI counts
567 per cell. Cell clusters were visualized using dimensionality reduction tool,
568 namely uniform manifold approximation and projection (UMAP). The statistical

569 significance was performed using Wilcox test.

570

571 **Cells**

572 HT29 cells were purchased from American Type Culture Collection (ATCC) and
573 cultured in RPMI 1640 medium (Gibco) supplemented with 10% fetal bovine
574 serum (FBS) (Gibco), 1% penicillin and streptomycin (HyClone) at 37°C and 5%
575 CO₂. HEK293T cells were purchased from ATCC and maintained in DMEM
576 medium (Gibco) containing 10% FBS, 1% penicillin and streptomycin at 37°C
577 and 5% CO₂. To construct Gab1-knockdown HT29 cell line, shGab1 cDNA were
578 constructed into the PLKO1-puro vector and packaged into lentiviruses. HT29
579 cells were infected with shGab1 lentivirus and then screened by puromycin.
580 For stimulation, cells were plated on six-well plates at 5 × 10⁵ cells per well
581 overnight and then pretreated with RIPK1 inhibitor Nec-1s (10 µM; Selleck
582 Chemicals) for 1 h. After that, cells were stimulated with T/S/Z mix [TNF-α, 50
583 ng/ml (Novoprotein); SM-164, 50 nM (Selleck Chemicals); Z-VAD-FMK, 50 µM
584 (Selleck Chemicals)] for indicated time. Cell lysates and culture supernatant
585 were further analyzed by Western blot.

586

587 **GST fusion protein purification and pull-down assay**

588 Recombinant protein purification was performed as described previously (82).
589 Briefly, the GST tagged Gab1 full-length fusion proteins were expressed in E.
590 coli BL21 cells at 16 °C overnight to achieve maximal soluble expression. Cells
591 were harvested and lysed by sonication in lysis buffer (20 mM Tris-HCL PH 7.5,
592 300 mM NaCl, 1% Triton X-100 and Protease Inhibitor Cocktail), and then
593 centrifuged at 12,000 g for 15 min. Supernatant were collected and incubated
594 with glutathione-sepharose overnight at 4 °C. Total GST fusion protein
595 concentration was estimated by using BCA Protein Assay kit (Beyotime). 293T
596 cells were seeded onto 10-mm dishes transfected with full-length RIPK3
597 plasmids, and lysed with a lysis buffer (50 mM Tris-HCl, pH 7.4, 150 mM NaCl,
598 1% Triton X-100, 1% sodium deoxycholate, 0.1% SDS, 1 mM EDTA and

599 protease inhibitor cocktail). After centrifugation, cleared cell lysates were
600 incubated with purified GST-Gab1 beads or the control beads overnight at 4 °C
601 with gentle rotation. Then the glutathione beads were washed three times with
602 lysis buffer and eluted with loading buffer for Western blot analysis.

603

604 **Crypt isolation and organoid culture**

605 The intestinal organoids were derived from the small intestines as reported (24),
606 with slight modifications. In brief, 10-cm small intestines were dissected and
607 opened longitudinally to remove luminal contents. The intestine was cut into 5
608 mm pieces and incubated with 4 mM EDTA in PBS for 30 min at 4°C without
609 shaking. Crypts were dissociated from villi by pipetting and filtered through a
610 70-µm strainer, followed by centrifugation and washing. The purified crypts
611 were resuspended in Matrigel (Coring, 356231) and seeded onto glass-bottom
612 dish, and cultured in IntestiCult Organoid Growth Medium (StemCell, 06005).
613 Organoid growth medium was refreshed every 2-3 days. For the PI-traced
614 organoid cell-death assay, TNF-α (50 ng/ml) ,SM-164 (50 nM), Z-VAD-FMK (50
615 µM) were added into organoid growth medium for 8 h at day 7. Then organoids
616 were stained with 1 µg/ml PI and images were taken using a confocal
617 microscope (FV3000, Olympus).

618

619 **Statistics**

620 Data are presented as mean ± SEM and statistical calculations were performed
621 with GraphPad Prism 8.0. Statistical analysis was performed using two-tailed
622 unpaired Student's t-test (for two group comparison), one-way or two-way
623 ANOVA followed by multi-comparisons (for multiple group comparison). P< 0.05
624 was considered statistically significant.

625

626 **Study approval**

627 For human samples, written informed consent was obtained from all individuals
628 and all samples were deidentified. These studies were approved by the Medical

629 Ethics Committee of Sir Run Run Shaw Hospital. All animal experiments were
630 carried out in accordance with protocols approved by the Animal Care and Use
631 Committee of the Zhejiang University School of Medicine.

632

633 **Author contributions**

634 JX, ZJ and XZ conceived of and designed the project. JX, SL and WJ performed
635 experiments. JX and SL analyzed and interpreted data. HZ and XC performed
636 bioinformatic analyses. TZ and YF were in charge of recruiting patients/controls
637 and collected tissue samples. JX, YK and XZ wrote the manuscript and
638 designed figures. PX, HC, DW and ZJ edited the manuscript. All authors
639 approved the final manuscript.

640

641 **Acknowledgements**

642 The authors thank Prof. Gen-Sheng Feng (Department of Pathology, Division
643 of Biological Sciences and Moores Cancer Center, University of California, San
644 Diego, CA, USA) for providing the Gab1^{flox/flox} mice; Prof. Wenlong Lin (Zhejiang
645 University, Hangzhou, China) for critical suggestion to the experimental design.
646 We thank Xueping Zhou (Laboratory Animal Center, Zhejiang University,
647 Hangzhou, China) for mouse care; Shuangshuang Liu and Zhaoxiaonan Lin
648 (Core Facilities, Zhejiang University School of Medicine, Hangzhou, China) for
649 assistance with confocal microscopy; and Chengyu Yang (Center of Cryo-
650 Electron Microscopy, Zhejiang University, Hangzhou, China) for technical
651 support on TEM. This work was supported by the National Natural Science
652 Foundation of China (81800459 to JX).

653

654

655

656

657

658

659 **References**

- 660 1. Chang, J.T. 2020. Pathophysiology of Inflammatory Bowel Diseases. *N Engl J Med* 383:2652-2664.
- 661 2. Graham, D.B., et al. 2020. Pathway paradigms revealed from the genetics of inflammatory bowel disease. *Nature* 578:527-539.
- 662 3. Juznic, L., et al. 2021. SETDB1 is required for intestinal epithelial differentiation and the prevention of intestinal inflammation. *Gut* 70:485-498.
- 663 4. Spalinger, M.R., et al. 2020. PTPN2 Regulates Interactions Between Macrophages and Intestinal Epithelial Cells to Promote Intestinal Barrier Function. *Gastroenterology* 159:1763-1777 e1714.
- 664 5. Kumar, A., et al. 2021. A Novel Role of SLC26A3 in the Maintenance of Intestinal Epithelial Barrier Integrity. *Gastroenterology* 160:1240-1255 e1243.
- 665 6. Bai, R., et al. 2020. Myeloid cells protect intestinal epithelial barrier integrity through the angiogenin/plexin-B2 axis. *EMBO J* 39:e103325.
- 666 7. Peterson, L.W., et al. 2014. Intestinal epithelial cells: regulators of barrier function and immune homeostasis. *Nat Rev Immunol* 14:141-153.
- 667 8. Martens, E.C., et al. 2018. Interactions of commensal and pathogenic microorganisms with the intestinal mucosal barrier. *Nat Rev Microbiol* 16:457-470.
- 668 9. Martini, E., et al. 2017. Mend Your Fences: The Epithelial Barrier and its Relationship With Mucosal Immunity in Inflammatory Bowel Disease. *Cell Mol Gastroenterol Hepatol* 4:33-46.
- 669 10. Mehandru, S., et al. 2021. The intestinal barrier, an arbitrator turned provocateur in IBD. *Nat Rev Gastroenterol Hepatol* 18:83-84.
- 670 11. Patankar, J.V., et al. 2020. Cell death in the gut epithelium and implications for chronic inflammation. *Nat Rev Gastroenterol Hepatol* 17:543-556.
- 671 12. Gunther, C., et al. 2013. Apoptosis, necrosis and necroptosis: cell death

- 689 regulation in the intestinal epithelium. *Gut* 62:1062-1071.
- 690 13. Pasparakis, M., et al. 2015. Necroptosis and its role in inflammation.
691 *Nature* 517:311-320.
- 692 14. Patankar, J.V., et al. 2021. E-type prostanoid receptor 4 drives resolution
693 of intestinal inflammation by blocking epithelial necroptosis. *Nat Cell Biol*
694 23:796-807.
- 695 15. Xie, Y., et al. 2020. Gut epithelial TSC1/mTOR controls RIPK3-
696 dependent necroptosis in intestinal inflammation and cancer. *J Clin*
697 *Invest* 130:2111-2128.
- 698 16. Kearney, C.J., et al. 2017. An Inflammatory Perspective on Necroptosis.
699 *Mol Cell* 65:965-973.
- 700 17. Choi, M.E., et al. 2019. Necroptosis: a crucial pathogenic mediator of
701 human disease. *JCI Insight* 4.
- 702 18. Wang, H.Y., et al. 2014. Mixed Lineage Kinase Domain-like Protein
703 MLKL Causes Necrotic Membrane Disruption upon Phosphorylation by
704 RIP3. *Molecular Cell* 54:133-146.
- 705 19. Kaczmarek, A., et al. 2013. Necroptosis: the release of damage-
706 associated molecular patterns and its physiological relevance. *Immunity*
707 38:209-223.
- 708 20. He, S., et al. 2009. Receptor interacting protein kinase-3 determines
709 cellular necrotic response to TNF-alpha. *Cell* 137:1100-1111.
- 710 21. Sun, L., et al. 2012. Mixed lineage kinase domain-like protein mediates
711 necrosis signaling downstream of RIP3 kinase. *Cell* 148:213-227.
- 712 22. Gunther, C., et al. 2011. Caspase-8 regulates TNF-alpha-induced
713 epithelial necroptosis and terminal ileitis. *Nature* 477:335-339.
- 714 23. Welz, P.S., et al. 2011. FADD prevents RIP3-mediated epithelial cell
715 necrosis and chronic intestinal inflammation. *Nature* 477:330-334.
- 716 24. Wang, R., et al. 2020. Gut stem cell necroptosis by genome instability
717 triggers bowel inflammation. *Nature* 580:386-390.
- 718 25. Pierdomenico, M., et al. 2014. Necroptosis Is Active in Children With

- 719 Inflammatory Bowel Disease and Contributes to Heighten Intestinal
720 Inflammation. *American Journal of Gastroenterology* 109:279-287.
- 721 26. Zhou, M., et al. 2021. ABIN3 Negatively Regulates Necroptosis-induced
722 Intestinal Inflammation Through Recruiting A20 and Restricting the
723 Ubiquitination of RIPK3 in Inflammatory Bowel Disease. *J Crohns Colitis*
724 15:99-114.
- 725 27. HolgadoMadruga, M., et al. 1996. A Grb2-associated docking protein in
726 EGF- and insulin-receptor signalling. *Nature* 379:560-564.
- 727 28. Weidner, K.M., et al. 1996. Interaction between Gab1 and the c-Met
728 receptor tyrosine kinase is responsible for epithelial morphogenesis.
729 *Nature* 384:173-176.
- 730 29. Wang, K., et al. 2016. Epithelial disruption of Gab1 perturbs surfactant
731 homeostasis and predisposes mice to lung injuries. *Am J Physiol Lung
732 Cell Mol Physiol* 311:L1149-L1159.
- 733 30. Zhang, Y., et al. 2016. Scaffolding protein Gab1 regulates myeloid
734 dendritic cell migration in allergic asthma. *Cell Res* 26:1226-1241.
- 735 31. Guo, X., et al. 2017. Increased levels of Gab1 and Gab2 adaptor proteins
736 skew interleukin-4 (IL-4) signaling toward M2 macrophage-driven
737 pulmonary fibrosis in mice. *J Biol Chem* 292:14003-14015.
- 738 32. Kizu, T., et al. 2015. Loss of Gab1 adaptor protein in hepatocytes
739 aggravates experimental liver fibrosis in mice. *Am J Physiol Gastrointest
740 Liver Physiol* 308:G613-624.
- 741 33. Zhao, J., et al. 2016. Cardiac Gab1 deletion leads to dilated
742 cardiomyopathy associated with mitochondrial damage and
743 cardiomyocyte apoptosis. *Cell Death Differ* 23:695-706.
- 744 34. Vancamelbeke, M., et al. 2017. Genetic and Transcriptomic Bases of
745 Intestinal Epithelial Barrier Dysfunction in Inflammatory Bowel Disease.
746 *Inflamm Bowel Dis* 23:1718-1729.
- 747 35. Parikh, K., et al. 2019. Colonic epithelial cell diversity in health and
748 inflammatory bowel disease. *Nature* 567:49-55.

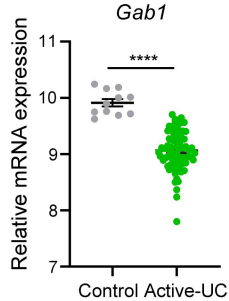
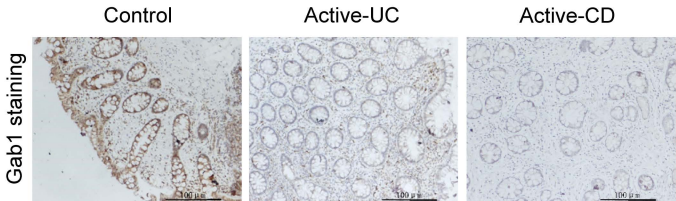
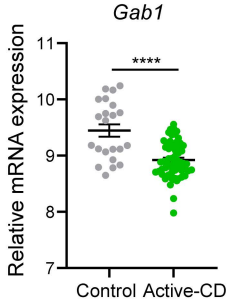
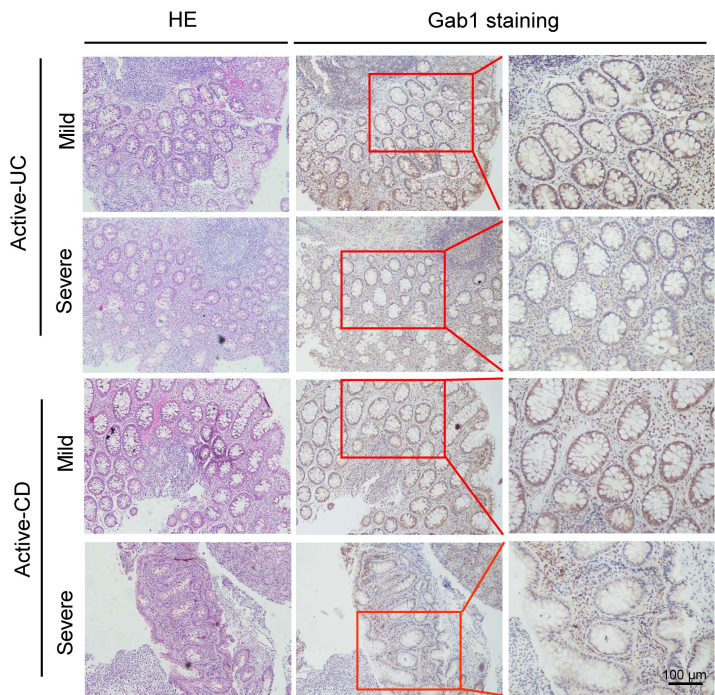
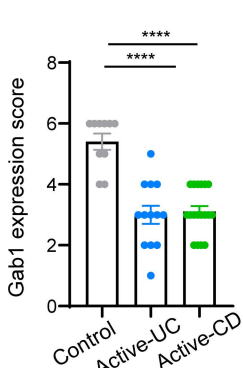
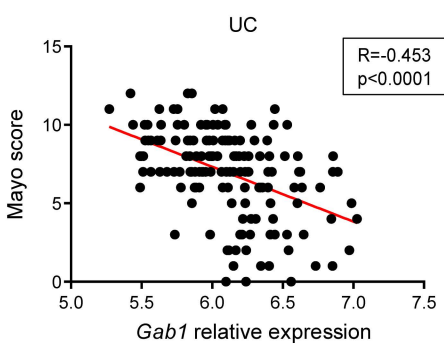
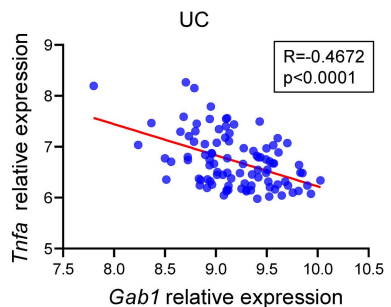
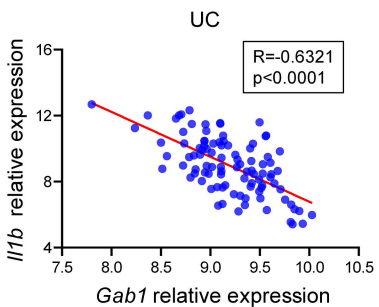
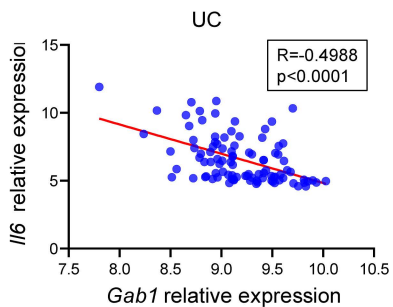
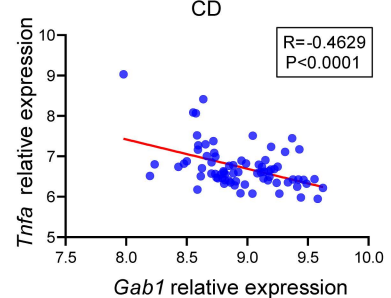
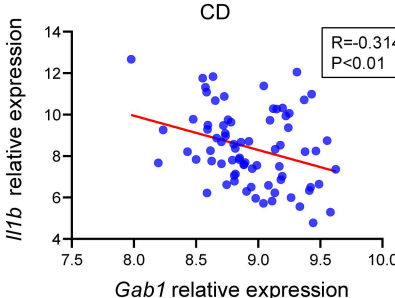
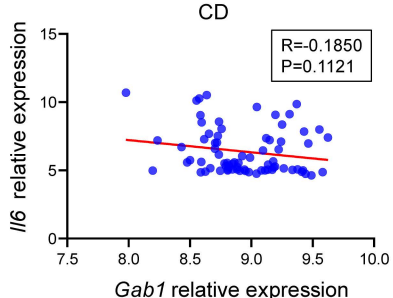
- 749 36. Langer, V., et al. 2019. IFN-gamma drives inflammatory bowel disease
750 pathogenesis through VE-cadherin directed vascular barrier disruption.
751 *Journal of Clinical Investigation* 129:4691-4707.
- 752 37. Marchiando, A.M., et al. 2011. The epithelial barrier is maintained by in
753 vivo tight junction expansion during pathologic intestinal epithelial
754 shedding. *Gastroenterology* 140:1208-1218 e1201-1202.
- 755 38. Newton, K., et al. 2021. Dying cells fan the flames of inflammation.
756 *Science* 374:1076-1080.
- 757 39. Lin, J., et al. 2016. RIPK1 counteracts ZBP1-mediated necroptosis to
758 inhibit inflammation. *Nature* 540:124-128.
- 759 40. Grootjans, S., et al. 2017. Initiation and execution mechanisms of
760 necroptosis: an overview. *Cell Death and Differentiation* 24:1184-1195.
- 761 41. Bar-Yoseph, H., et al. 2019. Infliximab-Tumor Necrosis Factor
762 Complexes Elicit Formation of Anti-Drug Antibodies. *Gastroenterology*
763 157:1338-1351 e1338.
- 764 42. Qiu, W., et al. 2011. PUMA-mediated intestinal epithelial apoptosis
765 contributes to ulcerative colitis in humans and mice. *J Clin Invest*
766 121:1722-1732.
- 767 43. Zhang, D., et al. 2022. TL1A/DR3 Axis, A Key Target of TNF-a, Augments
768 the Epithelial-Mesenchymal Transformation of Epithelial Cells in OVA-
769 Induced Asthma. *Front Immunol* 13:854995.
- 770 44. Zhu, S., et al. 2017. Nlrp9b inflammasome restricts rotavirus infection in
771 intestinal epithelial cells. *Nature* 546:667-+.
- 772 45. Patankar, J.V., et al. 2021. E-type prostanoid receptor 4 drives resolution
773 of intestinal inflammation by blocking epithelial necroptosis. *Nature Cell
774 Biology* 23:796-+.
- 775 46. Gunther, C., et al. 2015. Caspase-8 controls the gut response to
776 microbial challenges by Tnf-alpha-dependent and independent
777 pathways. *Gut* 64:601-610.
- 778 47. Sun, L.M., et al. 2012. Mixed Lineage Kinase Domain-like Protein

- 779 Mediates Necrosis Signaling Downstream of RIP3 Kinase. *Cell* 148:213-
780 227.
- 781 48. He, S.D., et al. 2009. Receptor Interacting Protein Kinase-3 Determines
782 Cellular Necrotic Response to TNF-alpha. *Cell* 137:1100-1111.
- 783 49. Xie, Y., et al. 2017. Inhibition of Aurora Kinase A Induces Necroptosis in
784 Pancreatic Carcinoma. *Gastroenterology* 153:1429-1443 e1425.
- 785 50. Lee, S.B., et al. 2019. The AMPK-Parkin axis negatively regulates
786 necroptosis and tumorigenesis by inhibiting the necrosome. *Nature Cell
787 Biology* 21:940-+.
- 788 51. Chen, J.X., et al. 2018. RIP3 dependent NLRP3 inflammasome
789 activation is implicated in acute lung injury in mice. *Journal of
790 Translational Medicine* 16.
- 791 52. Kennedy, N.A., et al. 2019. Predictors of anti-TNF treatment failure in
792 anti-TNF-naive patients with active luminal Crohn's disease: a
793 prospective, multicentre, cohort study. *Lancet Gastroenterology &
794 Hepatology* 4:341-353.
- 795 53. Xiao, P., et al. 2019. Phosphatase Shp2 exacerbates intestinal
796 inflammation by disrupting macrophage responsiveness to interleukin-
797 10. *J Exp Med* 216:337-349.
- 798 54. Rana, N., et al. 2022. GSDMB is increased in IBD and regulates
799 epithelial restitution/repair independent of pyroptosis. *Cell* 185:283-298
800 e217.
- 801 55. Healy, M.E., et al. 2020. MCL1 Is Required for Maintenance of Intestinal
802 Homeostasis and Prevention of Carcinogenesis in Mice.
803 *Gastroenterology* 159:183-199.
- 804 56. Ramos, G.P., et al. 2019. Mechanisms of Disease: Inflammatory Bowel
805 Diseases. *Mayo Clin Proc* 94:155-165.
- 806 57. Allaire, J.M., et al. 2018. The Intestinal Epithelium: Central Coordinator
807 of Mucosal Immunity. *Trends Immunol* 39:677-696.
- 808 58. Luissint, A.C., et al. 2016. Inflammation and the Intestinal Barrier:

- 809 Leukocyte-Epithelial Cell Interactions, Cell Junction Remodeling, and
810 Mucosal Repair. *Gastroenterology* 151:616-632.
- 811 59. Maloy, K.J., et al. 2011. Intestinal homeostasis and its breakdown in
812 inflammatory bowel disease. *Nature* 474:298-306.
- 813 60. Itoh, M., et al. 2000. Role of Gab1 in heart, placenta, and skin
814 development and growth factor- and cytokine-induced extracellular
815 signal-regulated kinase mitogen-activated protein kinase activation. *Mol
816 Cell Biol* 20:3695-3704.
- 817 61. Higuchi, K., et al. 2012. Endothelial Gab1 deletion accelerates
818 angiotensin II-dependent vascular inflammation and atherosclerosis in
819 apolipoprotein E knockout mice. *Circ J* 76:2031-2040.
- 820 62. Wang, Z., et al. 2019. Gab2 and Gab3 Redundantly Suppress Colitis by
821 Modulating Macrophage and CD8(+) T-Cell Activation. *Front Immunol*
822 10:486.
- 823 63. Lin, W., et al. 2017. Raf kinase inhibitor protein mediates intestinal
824 epithelial cell apoptosis and promotes IBDs in humans and mice. *Gut*
825 66:597-610.
- 826 64. Pochard, C., et al. 2021. PGI2 Inhibits Intestinal Epithelial Permeability
827 and Apoptosis to Alleviate Colitis. *Cell Mol Gastroenterol Hepatol*
828 12:1037-1060.
- 829 65. Xu, M., et al. 2020. Ferroptosis involves in intestinal epithelial cell death
830 in ulcerative colitis. *Cell Death Dis* 11:86.
- 831 66. Mayr, L., et al. 2020. Dietary lipids fuel GPX4-restricted enteritis
832 resembling Crohn's disease. *Nat Commun* 11:1775.
- 833 67. Jiao, H., et al. 2020. Z-nucleic-acid sensing triggers ZBP1-dependent
834 necroptosis and inflammation. *Nature* 580:391-395.
- 835 68. Werts, A.D., et al. 2020. A Novel Role for Necroptosis in the
836 Pathogenesis of Necrotizing Enterocolitis. *Cell Mol Gastroenterol
837 Hepatol* 9:403-423.
- 838 69. Furuta, K., et al. 2016. Gab1 Adaptor Protein Acts As a Gatekeeper to

- 839 Balance Hepatocyte Death and Proliferation During Acetaminophen-
840 Induced Liver Injury in Mice. *Hepatology* 63:1340-1355.
- 841 70. Weinlich, R., et al. 2017. Necroptosis in development, inflammation and
842 disease. *Nat Rev Mol Cell Biol* 18:127-136.
- 843 71. Chen, D., et al. 2018. PUMA amplifies necroptosis signaling by activating
844 cytosolic DNA sensors. *Proc Natl Acad Sci U S A* 115:3930-3935.
- 845 72. Seiden-Long, I., et al. 2008. Gab1 but not Grb2 mediates tumor
846 progression in Met overexpressing colorectal cancer cells.
847 *Carcinogenesis* 29:647-655.
- 848 73. Bai, R., et al. 2015. MicroRNA-409-3p suppresses colorectal cancer
849 invasion and metastasis partly by targeting GAB1 expression. *Int J
850 Cancer* 137:2310-2322.
- 851 74. Liang, W.K., et al. 2022. Microarray and bioinformatic analysis reveal the
852 parental genes of m6A modified circRNAs as novel prognostic
853 signatures in colorectal cancer. *Frontiers in Oncology* 12.
- 854 75. Lichtenstein, G.R., et al. 2005. Infliximab maintenance treatment
855 reduces hospitalizations, surgeries, and procedures in fistulizing Crohn's
856 disease. *Gastroenterology* 128:862-869.
- 857 76. Colombel, J.F., et al. 2010. Infliximab, Azathioprine, or Combination
858 Therapy for Crohn's Disease. *New England Journal of Medicine*
859 362:1383-1395.
- 860 77. Kennedy, N.A., et al. 2019. Predictors of anti-TNF treatment failure in
861 anti-TNF-naive patients with active luminal Crohn's disease: a
862 prospective, multicentre, cohort study. *Lancet Gastroenterol Hepatol*
863 4:341-353.
- 864 78. Martens, S., et al. 2020. Inhibitors Targeting RIPK1/RIPK3: Old and New
865 Drugs. *Trends Pharmacol Sci* 41:209-224.
- 866 79. Mifflin, L., et al. 2020. Receptor-interacting protein kinase 1 (RIPK1) as
867 a therapeutic target. *Nature Reviews Drug Discovery* 19:553-571.
- 868 80. Chen, H., et al. 2021. Use of the ulcerative colitis endoscopic index of

- severity and Mayo endoscopic score for predicting the therapeutic effect
of mesalazine in patients with ulcerative colitis. *Laparosc Endosc Robot Surg* 4: 33-39.
81. Daperno, M., et al. 2004. Development and validation of a new, simplified endoscopic activity score for Crohn's disease: the SES-CD. *Gastrointest Endosc* 60:505-512.
82. Zhang, Y.F., et al. 2021. Phosphatase Shp2 regulates biogenesis of small extracellular vesicles by dephosphorylating Syntenin. *Journal of Extracellular Vesicles* 10.
- 878
- 879
- 880
- 881
- 882
- 883
- 884
- 885
- 886
- 887
- 888
- 889
- 890
- 891
- 892
- 893
- 894
- 895
- 896
- 897
- 898

A**B****D****C****E****F****G**

899 **Figure 1. Decreased Gab1 expression in human IBD samples.**

900 **(A)** *Gab1* mRNA expression in patients with active UC (n = 74) and matched
901 normal controls (n = 11), active CD (n = 59) and matched normal controls (n =
902 22), revealed by analyzing a database of RNA-sequencing data (GEO
903 accession number GSE75214).

904 **(B-C)** Representative immunohistochemical (IHC) staining of *Gab1* in colonic
905 mucosa from patients with active UC (n = 13) or active CD (n = 18), and normal
906 controls (n = 10) . Scale bars, 100 μ m.

907 **(D)** Representative images showing hematoxylin-eosin (H&E) staining and
908 *Gab1* IHC staining in mild and severe IBD samples. n=3 for each group. Scale
909 bars, 100 μ m.

910 **(E)** Pearson's correlation analysis was performed between relative *Gab1*
911 expression and clinical mayo score from UC patients (n=162). R=-0.453, P <
912 0.0001. Data were collected from GEO database GSE92415.

913 **(F)** Pearson's correlation analysis between *Gab1* expression and pro-
914 inflammatory cytokine *Il1b*, *Il6* or *Tnfa* in colon biopsy samples from UC patients
915 (n=97). R=-0.4988, P < 0.0001 for *Il6*; R=-0.6321, P < 0.0001 for *Il1b*; R=-
916 0.4672, P < 0.0001 for *Tnfa*. Data were collected from GEO database
917 GSE75214.

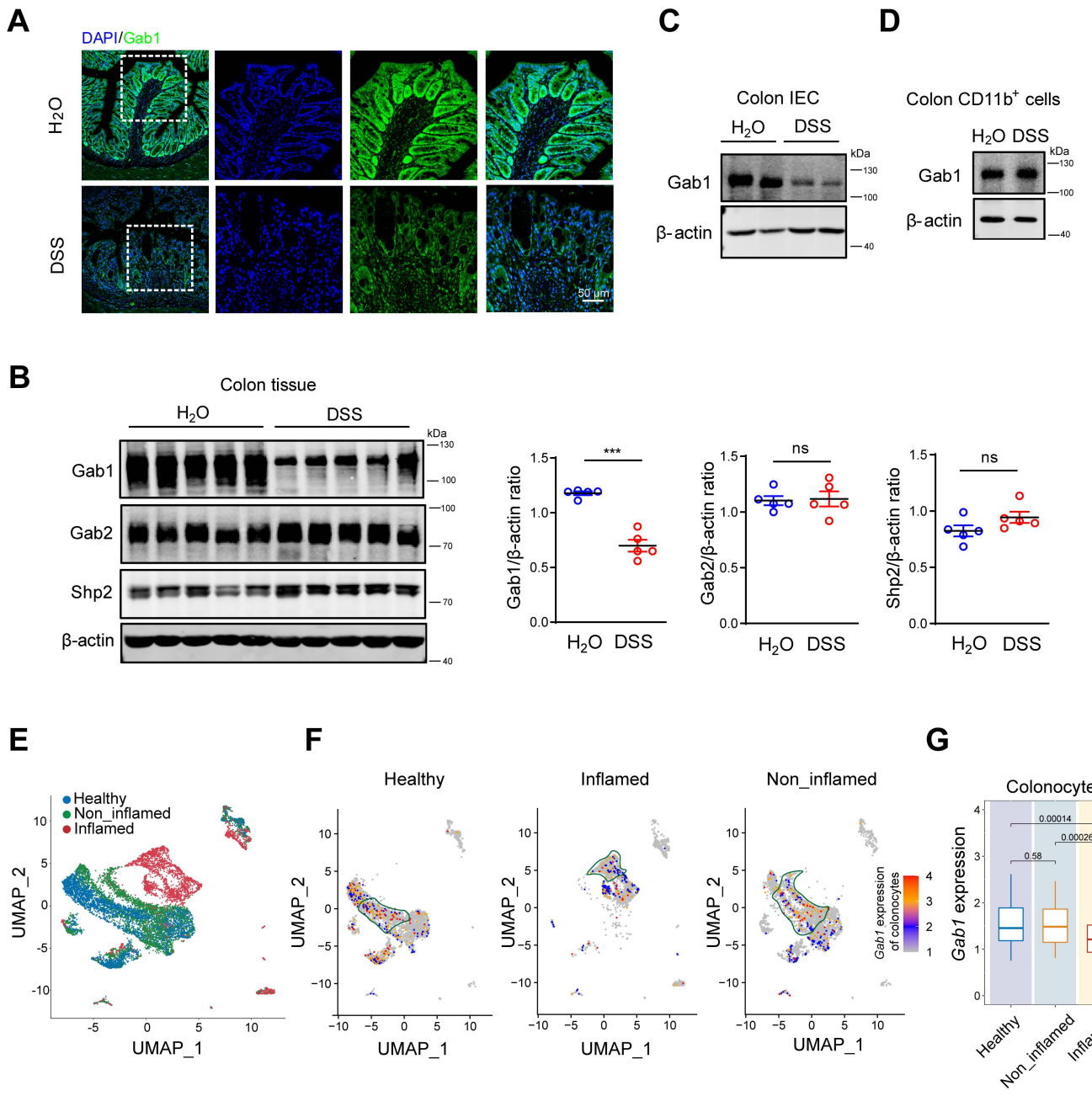
918 **(G)** Pearson's correlation analysis between *Gab1* expression and pro-
919 inflammatory cytokine *Il1b*, *Il6* or *Tnfa* in colon biopsy tissues from CD patients
920 (n=75). R=-0.1850, P=0.1121 for *Il6*; R=-0.3149, P < 0.01 for *Il1b*; R=-0.4629,
921 P < 0.0001 for *Tnfa*. Data were collected from GEO database GSE75214.

922 Quantitative data were shown as mean \pm SEM. Statistical significance was
923 assessed by using two-tailed Student's t-test (A), one-way ANOVA with multiple
924 comparisons test (C) and Pearson's correlation coefficient (E-G); **** p<0.0001;
925 ns, not significant. UC, ulcerative colitis; CD, Crohn's disease.

926

927

928



929 **Figure 2. Gab1 is decreased in IECs during mouse colitis and human UC.**
930 **(A)** Representative immunofluorescence staining for Gab1 (green) and DAPI
931 (blue) in mouse colons with or without a 7-day DSS treatment. Scale bars, 50
932 μ m.
933 **(B)** Western blotting of Gab1, Gab2 and Shp2 in mouse colonic tissues with or
934 without DSS treatment. Quantitative analyses were determined on the right.
935 n=5 for each group.
936 **(C)** Immunoblot analysis for Gab1 in IECs isolated from mouse colonic tissues
937 treated as described above. n=3 for each group.
938 **(D)** Immunoblot analysis for Gab1 in CD11b⁺ cells sorting from colonic lamina
939 propria (CLP) treated as described above. n=3 for each group.
940 **(E)** UMAP plots of single-cell clusters of colonic crypts from patients with
941 inflamed/non-inflamed UC and healthy controls (n = 3 per group) by analyzing
942 a single-cell sequencing database (GEO accession number GSE116222).
943 **(F-G)** UMAP results **(F)** depicting *Gab1* expression and distribution mapped to
944 referenced single-cell clusters (Fig S2C), with box plot **(G)** demonstrating *Gab1*
945 level in colonocytes of patients with inflamed/non-inflamed UC and healthy
946 controls (n = 3 per group) using the database as described above.
947 Quantitative data were shown as mean \pm SEM. Statistical significance was
948 assessed by using two-tailed Student's t-test (B) and Wilcox test (G);
949 ***p<0.001; ns, not significant. DSS, dextran sulfate sodium; IEC, intestinal
950 epithelial cell; UC, ulcerative colitis.

951

952

953

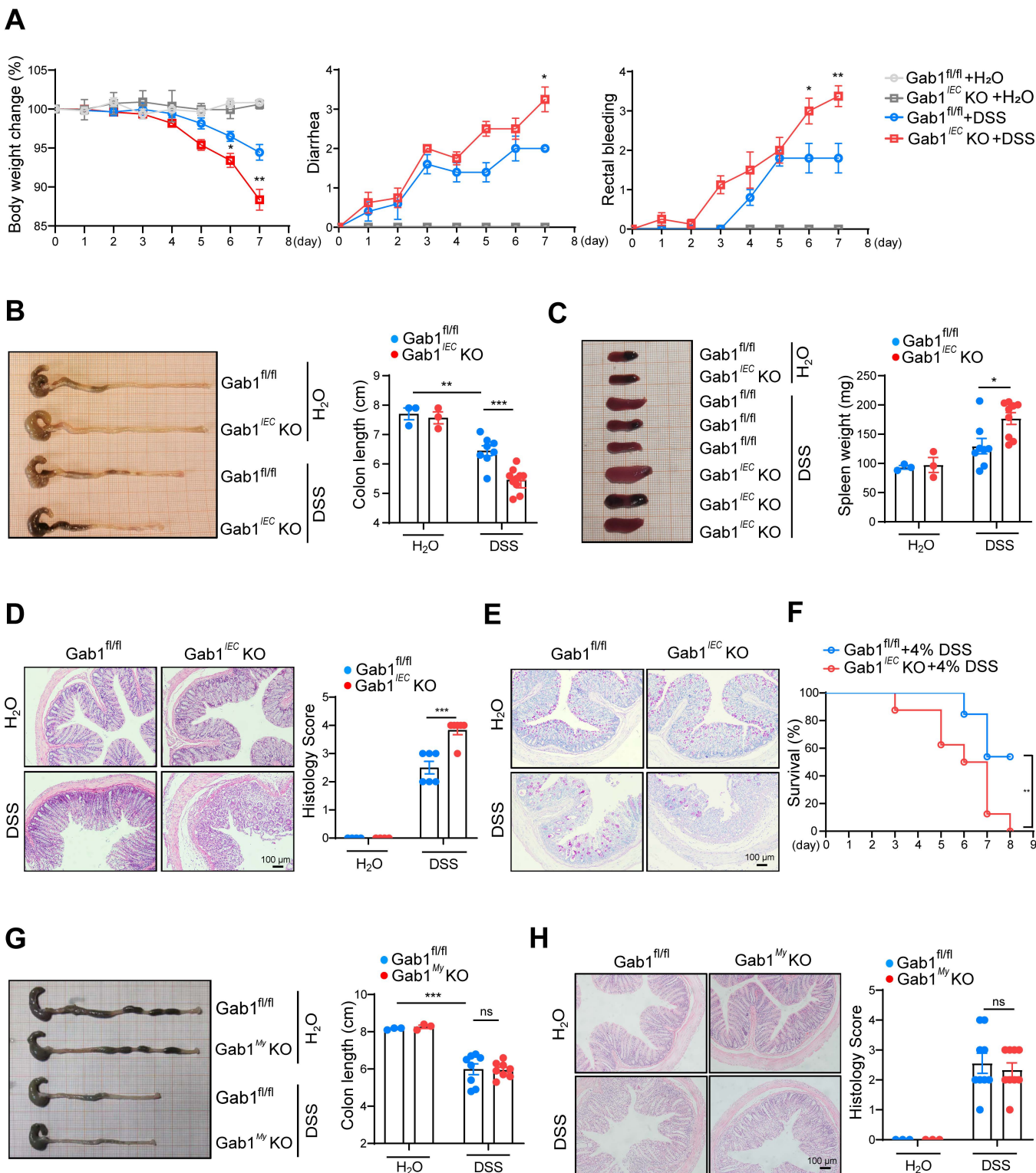
954

955

956

957

958



959 **Figure 3. Epithelial Gab1 deficiency enhances susceptibility to DSS-
960 induced experimental colitis.** Gab1^{IEC} KO mice (A-F) or Gab1^{My} KO mice (G-
961 H), as well as their littermates were administrated with water or 3% DSS for 7
962 days to induce experimental colitis.

963 **(A)** Body weight loss, diarrhea and rectal bleeding were monitored daily with
964 or without DSS treatment. n=3, 3, 8, 9, respectively.

965 **(B)** Gross morphology images of the colon from Gab1^{fl/fl} or Gab1^{IEC} KO mice,
966 and colon length were measured on day 7. n=3, 3, 8, 9, respectively.

967 **(C)** Gross morphology images of the spleen from Gab1^{fl/fl} or Gab1^{IEC} KO mice,
968 and spleen weight were assessed on day 7. n=3, 3, 8, 9, respectively.

969 **(D)** Representative images of H&E-stained colons from Gab1^{IEC} KO mice and
970 littermate controls, with histopathology analysis of colitis performed on day 7.
971 Scale bars, 100 µm. n=3, 3, 6, 6, respectively.

972 **(E)** Representative Periodic acid-Schiff (PAS) staining of colonic sections from
973 Gab1^{IEC} KO mice and littermate controls. Scale bars, 100 µm. n=3, 3, 6, 6,
974 respectively.

975 **(F)** Gab1^{fl/fl} (n=13) and Gab1^{IEC} KO (n=8) mice were challenged with 4% DSS
976 for 7 d, and the survival of mice was monitored.

977 **(G)** Gross morphology images of colons and colon length of Gab1^{fl/fl} and
978 Gab1^{My} KO mice. n=3, 3, 9, 9, respectively.

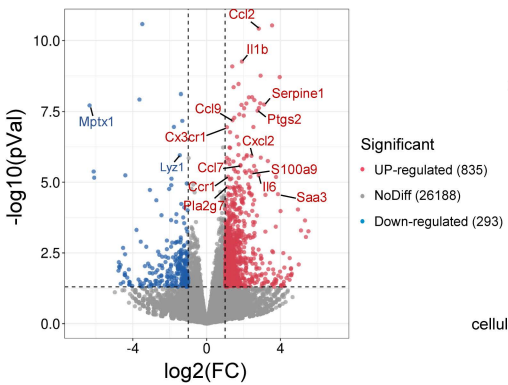
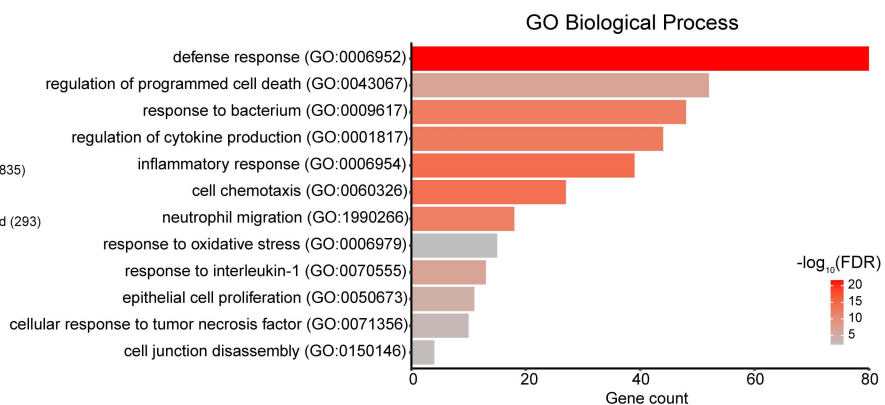
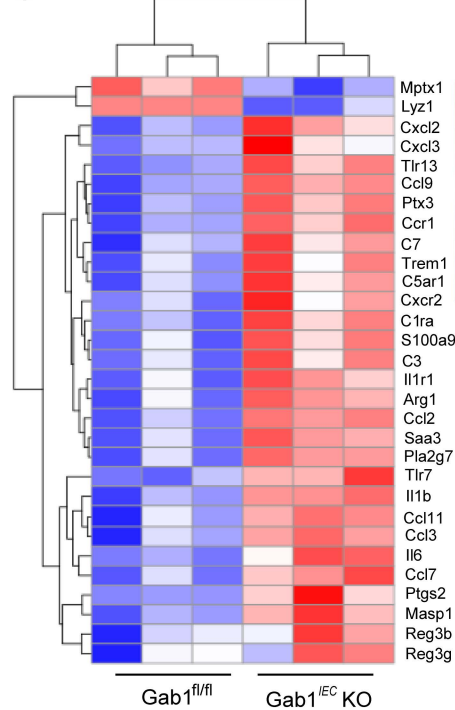
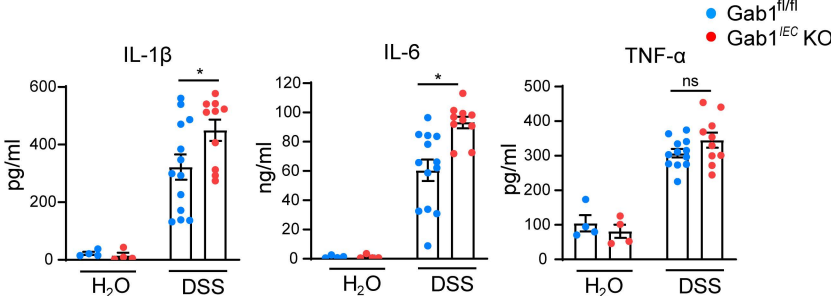
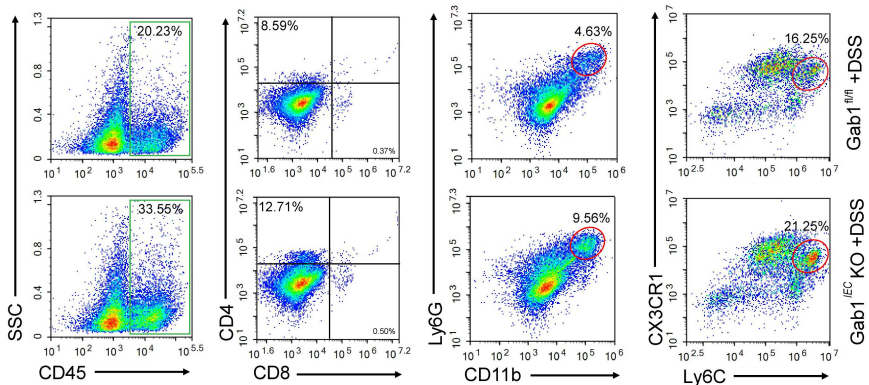
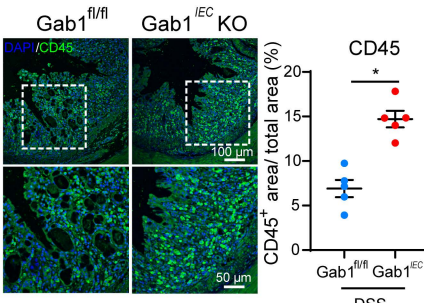
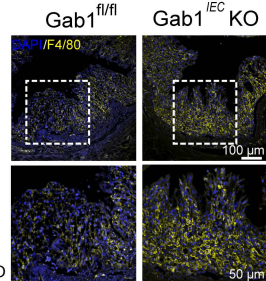
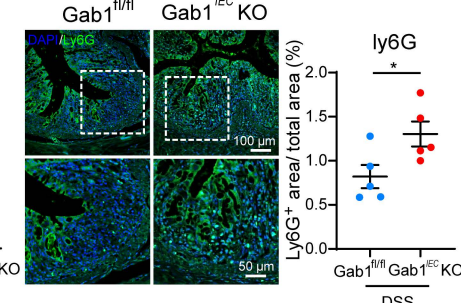
979 **(H)** Representative H&E staining and histopathological scores of colonic
980 sections from Gab1^{My} KO mice, as well as littermate controls. Scale bars, 100
981 µm. n=3, 3, 9, 9, respectively.

982 Quantitative data were shown as mean ± SEM and are representative of three
983 independent experiments. Statistical significance was assessed by using two-
984 way ANOVA with multiple comparisons test (A-D and G-H) and log-rank test (F);
985 *p<0.05, **p<0.01, ***p<0.001; ns, not significant.

986

987

988

A**B****C****D****E****F****G****H**

989 **Figure 4. Loss of Gab1 in IECs exacerbates inflammatory response in vivo.**

990 $\text{Gab1}^{\text{fl/fl}}$ and Gab1^{IEC} KO mice were challenged with 3% DSS and sacrificed at
991 day 7.

992 **(A)** Volcano plot of RNA-seq transcriptome data displaying the pattern of gene
993 expression values for epithelial Gab1-deficient colons relative to littermate
994 controls after DSS treatment. Red and blue dots, significantly up- and down-
995 regulated genes ($P < 0.05$, $|\log_2\text{FC}| > 1$). n=3 for each group.

996 **(B)** GO enrichment analysis classifying DEGs into biological process groups.

997 **(C)** Clustered heatmap showing expression changes of inflammation-
998 associated genes in epithelial Gab1-deficient colons versus littermate controls.
999 Red strip, high relative expression; blue strip, low relative expression. n=3 for
1000 each group.

1001 **(D)** Soluble cytokine levels in supernatant of cultured colonic tissue isolated
1002 from $\text{Gab1}^{\text{fl/fl}}$ and Gab1^{IEC} KO mice with or without DSS treatment. n = 4, 4, 13,
1003 10, respectively.

1004 **(E)** Representative flow cytometry plots of colon-infiltrated immune
1005 cells isolated from CLP at day 7. n = 3 for each group.

1006 **(F-H)** Representative immunofluorescence images stained for CD45 (green)
1007 (F), F4/80 (yellow) (G), Ly6G (green) (H) and DAPI (blue) from colon section
1008 with quantifications shown on the right. Scale bars, 100 μm (overview) and 50
1009 μm (magnification). n = 5 for each group.

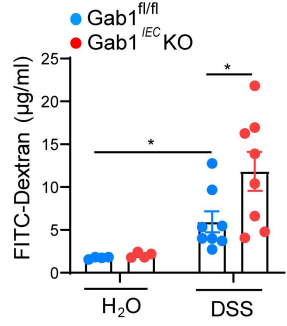
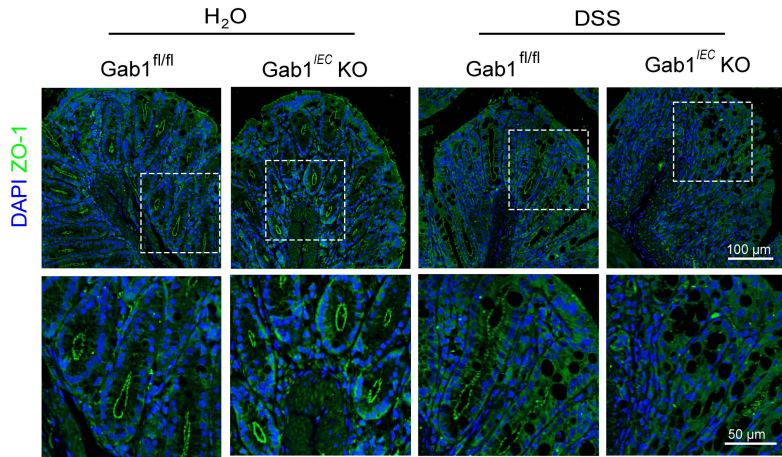
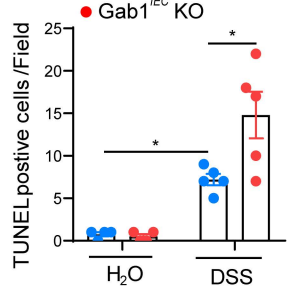
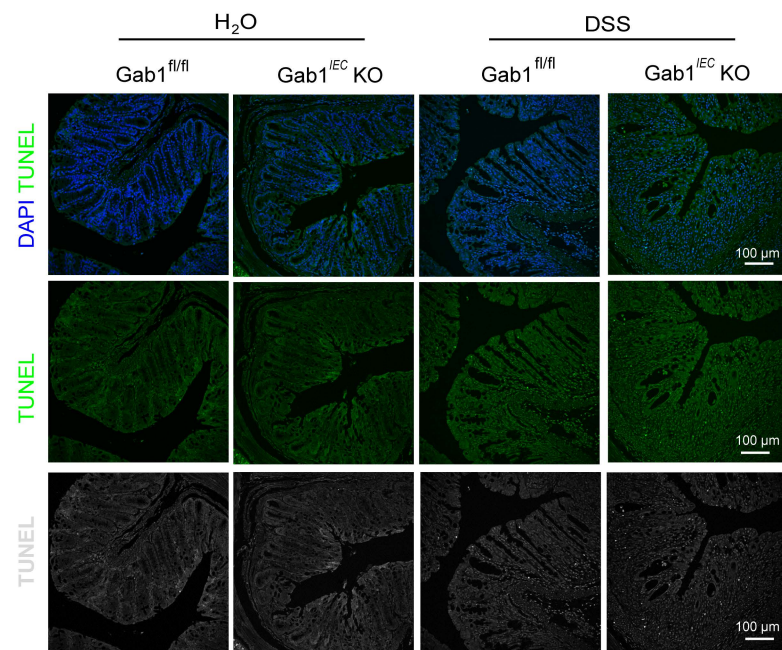
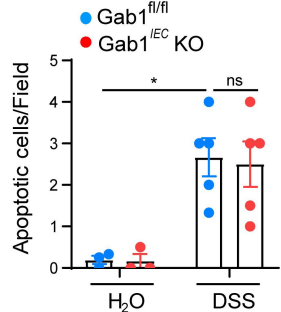
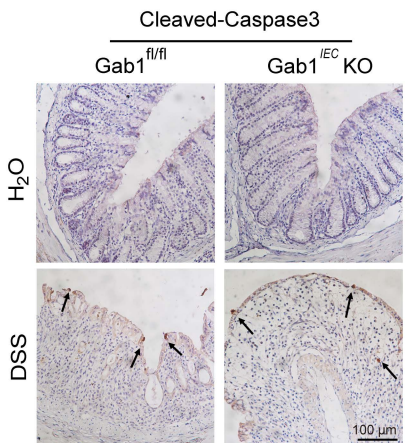
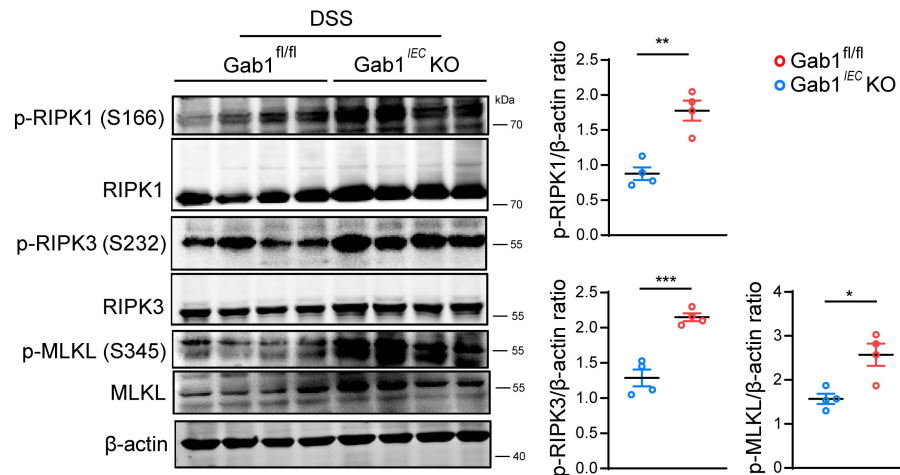
1010 Quantitative data were shown as mean \pm SEM. Statistical significance was
1011 assessed by using two-way ANOVA with multiple comparisons test (D) and two-
1012 tailed Student's t-test (F-H); * $p < 0.05$; ns, not significant. GO, gene ontology;
1013 DEGs, differentially-expressed genes; CLP, colonic lamina propria; SSC, side
1014 scatter.

1015

1016

1017

1018

A**B****D****C****E****F****G**

1019 **Figure 5. Gab1 maintains intestinal epithelial integrity through restricting**
1020 **aberrant necroptosis**

1021 **(A)** $\text{Gab1}^{\text{fl/fl}}$ and Gab1^{IEC} KO mice were administrated with 3% DSS for 7 d and
1022 fed with FITC-dextran intragastrically 4 hours before sacrifice, then serum
1023 FITC-dextran level was detected by fluorescence spectrophotometer. n=4, 4, 8,
1024 9, respectively.

1025 **(B)** Immunofluorescence staining of cell tight junction protein ZO-1 (green) and
1026 DAPI (blue) in colonic sections from the mice (n=5 per group) treated with DSS
1027 for 5 days. Arrows indicate the spatial arrangement of ZO-1 protein in luminal
1028 epithelium. Scale bars, 100 μm (overview) and 50 μm (magnification).

1029 **(C-D)** Representative images of TUNEL staining (green or grey) (C) and the
1030 quantifications of TUNEL $^{+}$ IECs in colonic sections on day 7 (D). n=4, 4, 5, 5,
1031 respectively. Scale bars, 100 μm .

1032 **(E-F)** Representative cleaved-caspase 3 IHC staining (F) and the number of
1033 apoptotic cells quantified (E) in colonic sections on day 7. Arrows indicate
1034 cleaved-caspase 3 positive cells. n=3, 3, 5, 5, respectively. Scale bars, 100 μm .

1035 **(G)** Immunoblots of colonic lysates following DSS treatment for 7 days on p-
1036 RIPK1 (S166), p-RIPK3 (S232) or p-MLKL (S345), and quantitative analyses
1037 were determined by Image J. n=4 for each group.

1038 Quantitative data were represented as mean \pm SEM. Statistical significance
1039 was performed by using two-way ANOVA with multiple comparisons test (A, D,
1040 E) and two-tailed Student's t-test (G); *p<0.05, **p<0.01, ***p<0.001; ns, not
1041 significant. FITC-dextran, fluorescein isothiocyanate-labeled dextran; TUNEL
1042 staining, eTdT-mediated dUTP nick-end labelling staining.

1043

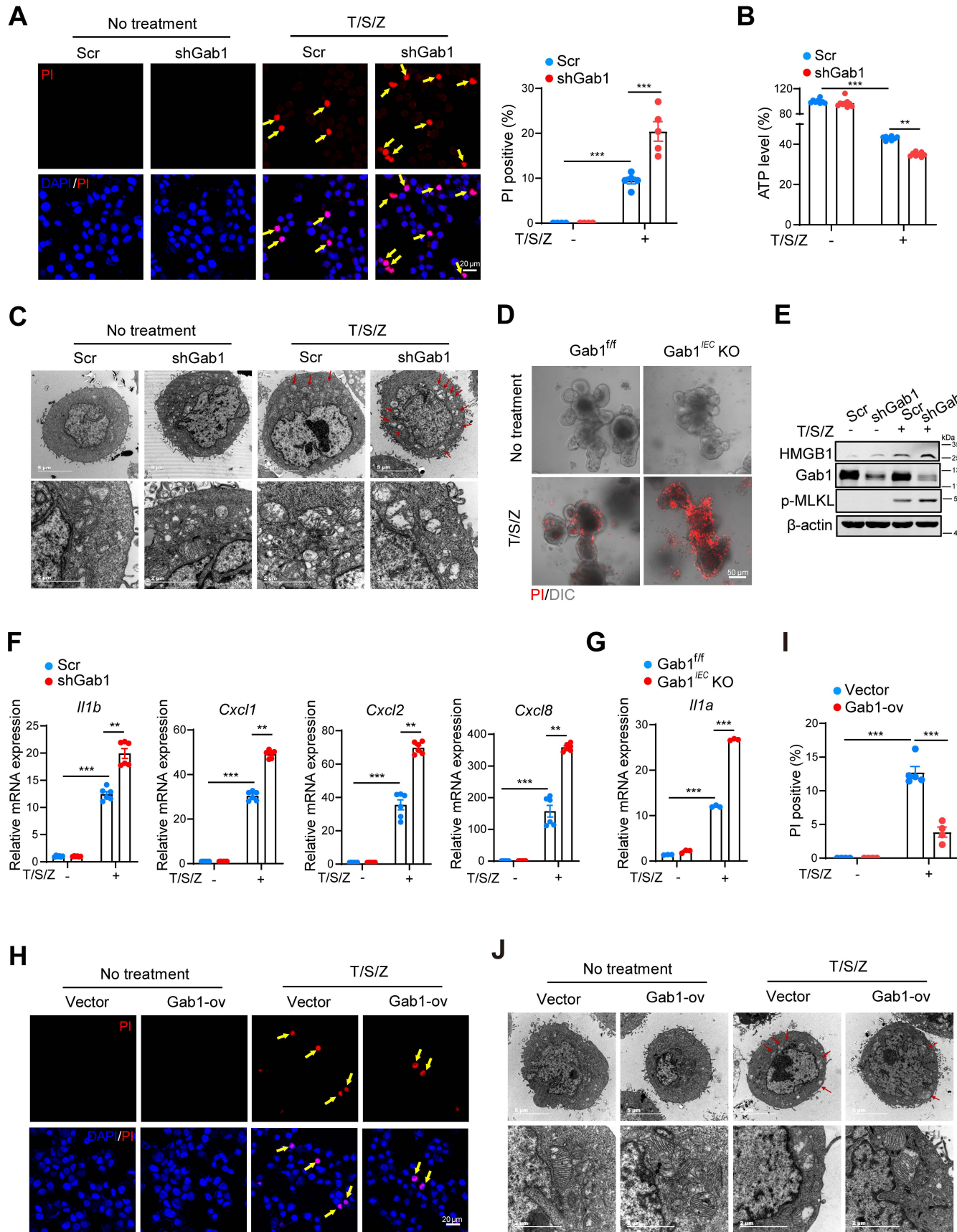
1044

1045

1046

1047

1048



1049 **Figure 6. Gab1 deficiency sensitizes IEC to T/S/Z induced necroptosis and**
1050 **inflammation**

1051 **(A)** Control (Scr) and Gab1-knockdown (shGab1) HT29 cells were treated with
1052 (n=5) or without (n=4) necrotic stimulation T/S/Z for 4 h, then stained with
1053 propidium iodide (PI) (red) and DAPI (blue). T/S/Z, TNF- α (50 ng/ mL), SM-164
1054 (50 ng/mL) and z-VAD (50 μ M). Scale bars, 20 μ m. Arrows indicated the cells
1055 undergoing necroptosis.

1056 **(B)** Viability of HT29 cells challenged with T/S/Z was determined by intracellular
1057 ATP levels using CellTiter-Glo® assays. n=8, 9, 8, 8, respectively.

1058 **(C)** Transmission electron microscopy (TEM) images showing the typical
1059 morphology of necroptosis in control (Scr) and Gab1-knockdown (shGab1)
1060 HT29 cells after T/S/Z treatment. Arrows pointed to the swelling mitochondria.
1061 Scale bars, 5 μ m (overview) and 2 μ m (magnification).

1062 **(D)** Representative confocal microscopy images of PI-stained intestinal
1063 organoids from Gab1^{f/f} and Gab1^{IEC} KO mice treated with T/S/Z for 8h. Scale
1064 bars, 50 μ m.

1065 **(E)** Western blot displaying the release of HMGB1 protein in the supernatant
1066 from control (Scr) and Gab1-knockdown (shGab1) HT29 cells treated with
1067 T/S/Z. Gab1, p-MLKL (S358) and β -actin were immunoblotted in cell lysates,
1068 respectively.

1069 **(F)** Quantitative mRNA expression of *Il1b*, *Cxcl1*, *Cxcl2* and *Cxcl8* in control
1070 (Scr) and Gab1-knockdown (shGab1) HT29 cells upon T/S/Z treatment. n=6 for
1071 each group.

1072 **(G)** Quantitative mRNA expression of *Il1a* in intestinal organoids from Gab1^{f/f}
1073 and Gab1^{IEC} KO mice upon T/S/Z treatment. n=3 for each group.

1074 **(H-I)** HT29 cells were transfected with pXJ40-Flag vector or pXJ40-Gab1-Flag
1075 followed by T/S/Z stimulation as in Fig 6A, then stained with PI (red) and DAPI
1076 (blue). Scale bars, 20 μ m. Arrows indicated the cells undergoing necroptosis. n
1077 = 4, 4, 5, 4, respectively.

1078 **(J)** Representative TEM images for the typical morphology of necroptosis in

1079 control (Vector) and Gab1-overexpressed (Gab1-ov) HT29 cells. Arrows
1080 indicated the swelling mitochondria. Scale bars, 5 μ m (overview) and 2 μ m
1081 (magnification).

1082 Data were represented as mean \pm SEM. All samples were biologically
1083 independent and three or more independent experiments were performed.
1084 Statistical significance was performed by using two-way ANOVA with multiple
1085 comparisons test (A, B, F, G, I); * p <0.05, ** p <0.01, *** p <0.001.

1086

1087

1088

1089

1090

1091

1092

1093

1094

1095

1096

1097

1098

1099

1100

1101

1102

1103

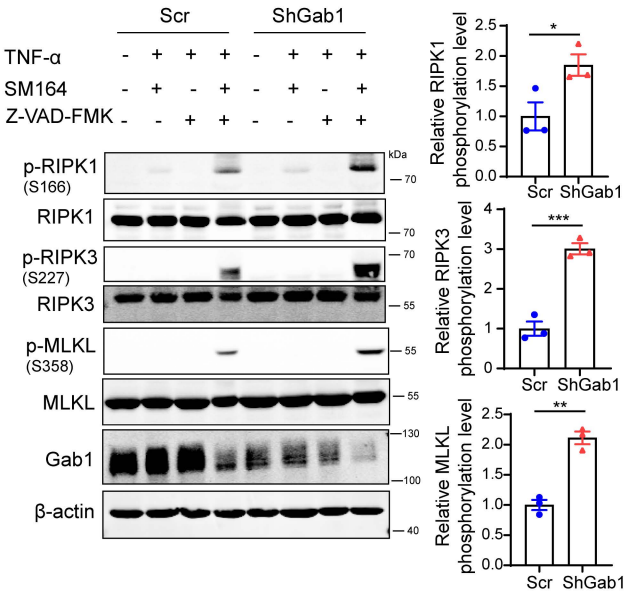
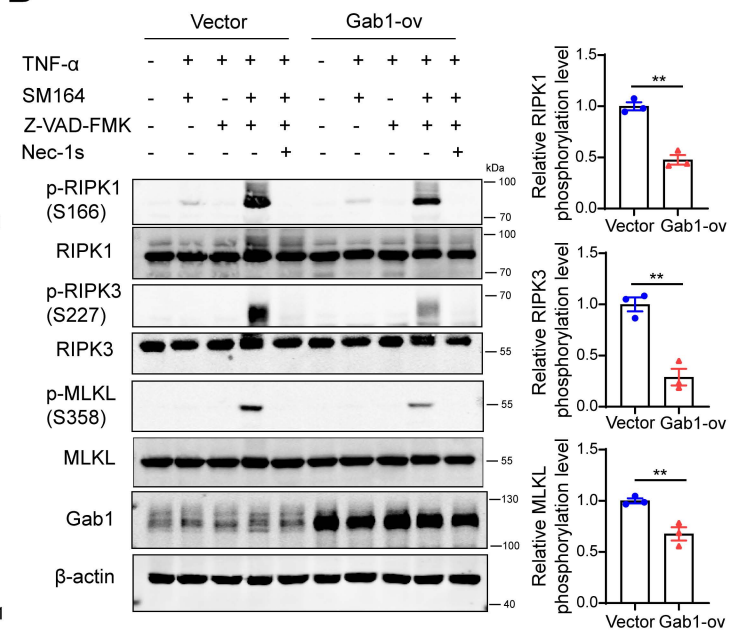
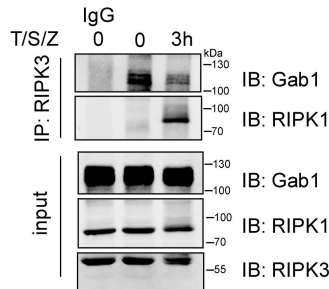
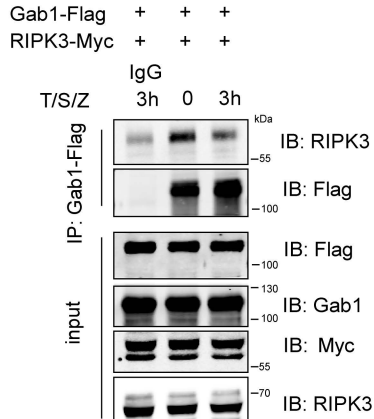
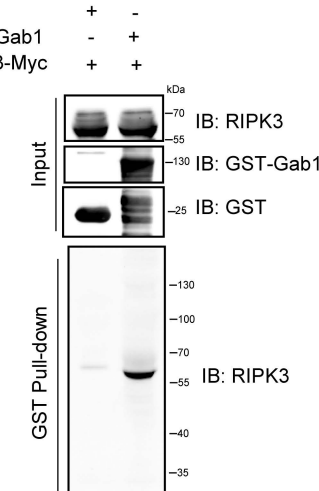
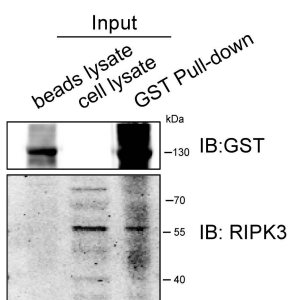
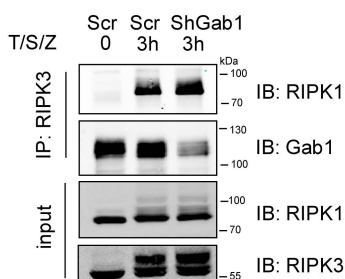
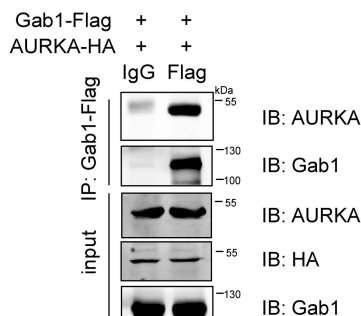
1104

1105

1106

1107

1108

A**B****C****D****E****F****G****H**

1109 **Figure 7. Gab1 blocks T/S/Z induced necroptosis via binding with RIPK3**

1110 **(A)** Control or Gab1-knockdown HT29 cells were treated with DMSO,
1111 TNF α +SM164, TNF α +Z-VAD-FMK or T/S/Z for 3 h, and phosphorylation of
1112 RIPK1, RIPK3, MLKL was determined by Western blotting. Quantitative data
1113 were shown as mean \pm SEM for three independent experiments.

1114 **(B)** Control or Gab1-overexpressed HT29 cells were pre-incubated with 10 μ m
1115 Nec-1s for 1 h, followed by DMSO, TNF α +SM164, TNF α +Z-VAD-FMK or T/S/Z
1116 treatment for 3 h. Detection of indicated proteins was carried out by Western
1117 blotting. Quantitative data were shown as mean \pm SEM for three independent
1118 experiments.

1119 **(C)** HT29 cells were treated with T/S/Z for 3 h. Total cell lysates were subjected
1120 to immunoprecipitation (IP) with anti-RIPK3 antibody or anti-IgG, followed by
1121 immunoblotting analysis with anti-Gab1 antibody, anti-RIPK1 antibody.

1122 **(D)** HEK293T cells were co-transfected with Gab1-Flag and RIPK3-Myc for 24
1123 h, followed by T/S/Z simulation for 3 h. Cell lysates were then subjected to IP
1124 using anti-Flag antibody or anti-IgG and immunoblotted as indicated.

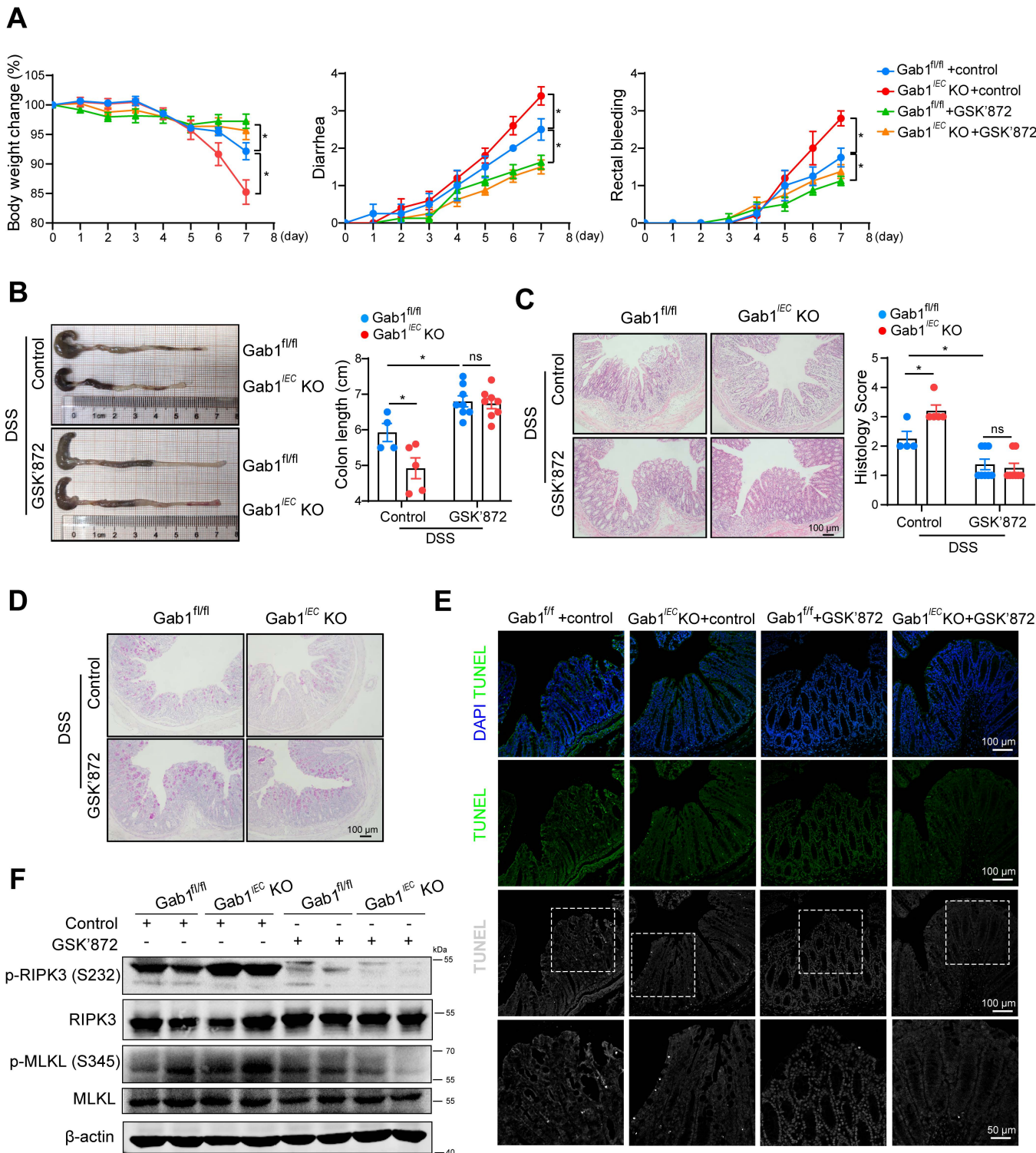
1125 **(E-F)** HEK293T were lysed and the supernatant were used to carry out a GST
1126 pull down assay to detect the interaction between Gab1 and RIPK3.
1127 Recombinant GST-fused Gab1 protein was incubated with HEK293T cell
1128 lysates with (E) or without RIPK3 overexpression (F), and analyzed by
1129 immunoblotting with the anti-RIPK3 antibody.

1130 **(G)** Western blot showing co-IP assay for RIPK1 and RIPK3 interaction in
1131 control or Gab1-knockdown HT29 cells after exposure to T/S/Z for 3 h.

1132 **(H)** HEK293T cells were co-transfected with Gab1-Flag and AURKA-HA for 24
1133 h. Total cell lysates were subjected to IP using anti-Flag antibody or anti-IgG,
1134 then immunoblotted with indicated antibodies.

1135 All samples were biologically independent and three independent experiments
1136 were performed. Statistical analysis was performed using two-tailed Student's
1137 t-test; *p<0.05, **p<0.01, ***p<0.001.

1138



1139 **Figure 8. Selective RIPK3 inhibitor GSK'872 rescued epithelial Gab1-**
1140 **deficient mice from DSS-induced colitis.** Gab1^{f/f} and Gab1^{IEC} KO mice were
1141 exposed to 3% DSS in drinking water as previously described, and
1142 intraperitoneally (i.p.) treated with either the vehicle control or GSK'872 at a
1143 dose of 10 mg/kg body weight once daily throughout the entire experimental
1144 period. n = 4, 5, 8, 8, respectively.

1145 **(A)** Relative percent change in body weight, as well as diarrhea and rectal
1146 bleeding scores were assessed daily.

1147 **(B)** Gross morphology images of the colon from Gab1^{f/f} and Gab1^{IEC} KO mice
1148 with different treatment. The colon length were measured on day 7.

1149 **(C)** Representative H&E-stained images and histological scores of the distal
1150 colon were assessed on day 7. Scale bars, 100 µm.

1151 **(D)** Representative PAS staining of colon sections from mice sacrificed at day
1152 7. Scale bars, 100 µm.

1153 **(E)** Representative images of TUNEL staining (green or grey) of colonic
1154 sections on day 7. Scale bars, 100 µm (overview) and 50 µm (magnification).

1155 **(F)** Immunoblotting of colonic protein from the DSS-challenged mice with or
1156 without GSK'872 administration on day 7.

1157 Quantitative data were presented as the mean ± SEM. Statistical analysis was
1158 performed by two-way ANOVA with multiple comparisons test; *p<0.05; ns,
1159 not significant. TUNEL staining, eTdT-mediated dUTP nick-end labelling
1160 staining.

1161

1162

1163

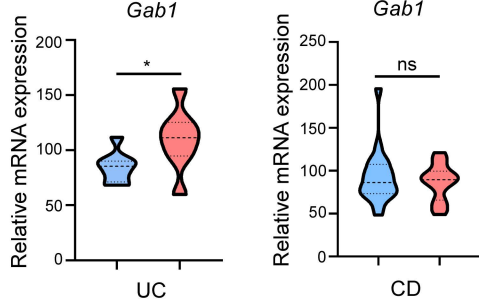
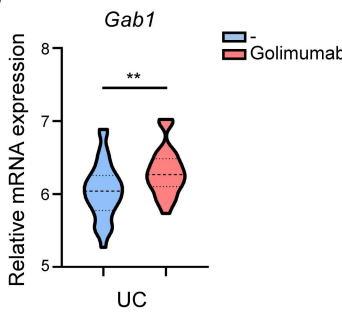
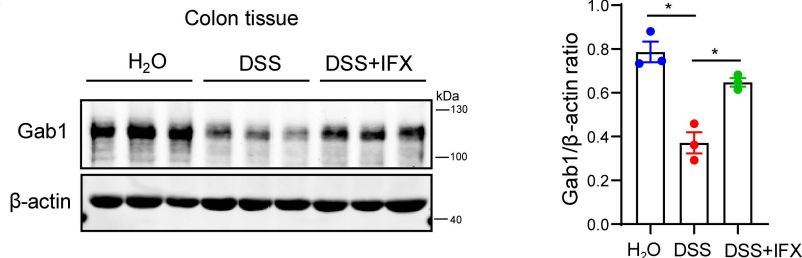
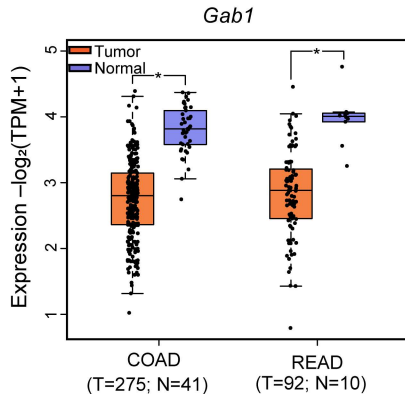
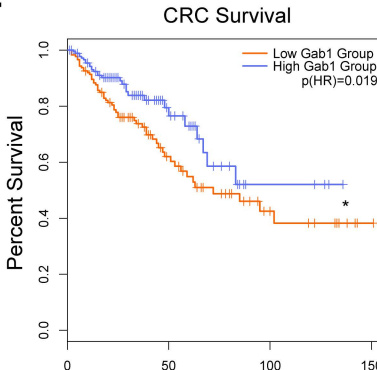
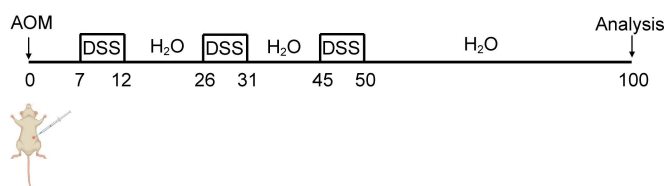
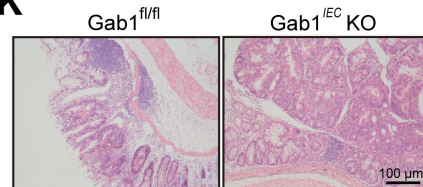
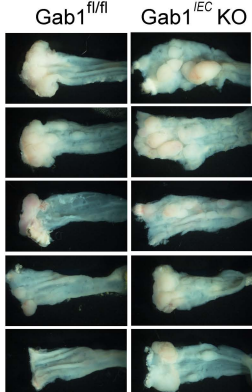
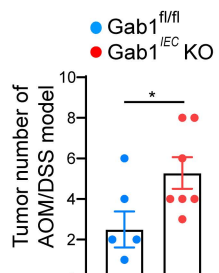
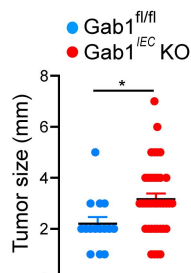
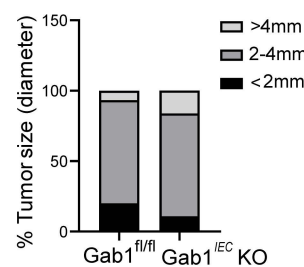
1164

1165

1166

1167

1168

A**B****C****D****E****F****K****G****H****I****J**

1169 **Figure 9. The clinical relevance of epithelial Gab1 in IBD treatment and**
1170 **colorectal cancer.**

1171 **(A)** *Gab1* mRNA expression in colon biopsies from infliximab-responded UC
1172 and CD patients before or after first infliximab induction. The data was obtained
1173 from GEO database GSE16879.

1174 **(B)** *Gab1* mRNA expression in colon biopsies from golimumab-responded UC
1175 patients before or after first golimumab induction. The data was obtained from
1176 GEO database GSE92415.

1177 **(C)** Mice were subjected to a 7-day course of 3% DSS and treated with
1178 infliximab intraperitoneally at day 5. *Gab1* expression in colonic tissues was
1179 determined at day 10 by Western blotting, with quantifications shown on the
1180 right. n=3 for each group.

1181 **(D)** Relative expression of *Gab1* in colorectal cancer (including COAD and
1182 READ) and matched normal tissue samples from GEPIA-based TCGA
1183 database.

1184 **(E)** Kaplan-Meier plots of patients with CRC with high or low *Gab1* expression,
1185 the data was collected from GEPIA-based TCGA database.

1186 **(F)** Schematic model of AOM/DSS-induced colitis-associated colorectal cancer
1187 (CAC).

1188 **(G-J)** Colorectal tumors were photographed (G) and the number of tumors per
1189 mouse (H), tumor size (I) as well as tumor distribution (J) were measured for
1190 each group. n = 6, 7, respectively.

1191 **(K)** Representative H&E staining of colonic sections from *Gab1*^{fl/fl} and *Gab1*^{IEC}
1192 KO mice. n = 6, 7, respectively. Scale bar, 100 μm.

1193 Data are shown as mean± SEM; Statistical analysis was performed using two-
1194 tailed Student's t-test (A, B, D, H, I) and one-way ANOVA with multiple
1195 comparisons test (C); *p<0.05, **p<0.01; ns, not significant. COAD: colon
1196 adenocarcinoma; READ: rectal adenocarcinoma; CRC: colorectal cancer;
1197 TCGA: The Cancer Genome Atlas; AOM: azoxymethane.

1198